Colloquium: Annual modulation of dark matter

Katherine Freese*

Michigan Center for Theoretical Physics, Department of Physics, University of Michigan, Ann Arbor, Michigan 48109, USA and Physics Department, Caltech, Pasadena, California 91101, USA

Mariangela Lisanti†

Princeton Center for Theoretical Science, Princeton University, Princeton, New Jersey 08544, USA

Christopher Savage‡

The Oskar Klein Centre for Cosmoparticle Physics, Department of Physics, Stockholm University, AlbaNova, SE-106 91 Stockholm, Sweden and Department of Physics & Astronomy, University of Utah, Salt Lake City, Utah 84112, USA

(published 1 November 2013)

Direct detection experiments, which are designed to detect the scattering of dark matter off nuclei in detectors, are a critical component in the search for the Universe's missing matter. This Colloquium begins with a review of the physics of direct detection of dark matter, discussing the roles of both the particle physics and astrophysics in the expected signals. The count rate in these experiments should experience an annual modulation due to the relative motion of the Earth around the Sun. This modulation, not present for most known background sources, is critical for solidifying the origin of a potential signal as dark matter. The focus is on the physics of annual modulation, discussing the practical formulas needed to interpret a modulating signal. The dependence of the modulation spectrum on the particle and astrophysics models for the dark matter is illustrated. For standard assumptions, the count rate has a cosine dependence with time, with a maximum in June and a minimum in December. Well-motivated generalizations of these models, however, can affect both the phase and amplitude of the modulation. Shown is how a measurement of an annually modulating signal could teach us about the presence of substructure in the galactic halo or about the interactions between dark and baryonic matter. Although primarily a theoretical review, the current experimental situation for annual modulation and future experimental directions is briefly discussed.

DOI: 10.1103/RevModPhys.85.1561 PACS numbers: 95.35.+d, 12.60.−i, 95.30.Cq

CONTENTS

*ktfreese@umich.edu
†mlisanti@princeton.edu
‡savage@physics.utah.edu

I. INTRODUCTION

The Milky Way galaxy is known to be surrounded by a halo of dark matter whose composition remains a mystery. Only 5% of the Universe consists of ordinary atomic matter, while the remainder is 23% dark matter and 72% dark energy

(Komatsu *et al.*, 2011). Identifying the nature of this dark matter is the longest outstanding problem in all of modern physics, stemming back to observations in 1933 by Fritz Zwicky; he proposed the existence of "dunkle materie" (German for "dark matter") as a source of gravitational potential to explain rapid motions of galaxies in the Coma Cluster (Zwicky, 1937). Subsequently, others discovered flat rotation curves in disk galaxies, starting with Babcock (1939) and followed (more persuasively and with better data) by Rubin, Ford, and Kent (1970) and Roberts and Whitehurst (1975). Their results imply that the predominant constituent of mass inside galaxies must be nonluminous matter [see Sandage, Sandage, and Kristian (1975) and Faber and Gallagher (1979) for reviews].

A leading candidate for this dark matter is a weakly interacting massive particle (WIMP). The terminology refers to the fact that these particles undergo weak interactions in addition to feeling the effects of gravity, but do not participate in electromagnetic or strong interactions. WIMPs are electrically neutral and the average number of interactions with the human body is at most one per minute, even with billions passing through every second (Freese and Savage, 2012). The expected WIMP mass ranges from 1 GeV to 10 TeV. These particles, if present in thermal equilibrium in the early Universe, annihilate with one another so that a predictable number of them remain today. The relic density of these particles is

$$\Omega_\chi h^2 \sim (3 \times 10^{-26}\ \mathrm{cm}^3/\mathrm{s})/\langle \sigma v \rangle_{\mathrm{ann}}, \tag{1}$$

where Ω_χ is the fractional contribution of WIMPs to the energy density of the Universe. An annihilation cross section $\langle \sigma v \rangle_{\mathrm{ann}}$ of weak interaction strength automatically gives the right answer, near the value measured by the Wilkinson Microwave Anisotropy Probe (WMAP) (Komatsu *et al.*, 2011). This coincidence is known as the "WIMP miracle" and is why WIMPs are taken so seriously as dark matter candidates. Possibly the best WIMP candidate is motivated by supersymmetry (SUSY): the lightest neutralino in the minimal supersymmetric standard model (MSSM) and its extensions (Jungman, Kamionkowski, and Griest, 1996). However, other WIMP candidates arise in a variety of theories beyond the standard model [see Bergstrom (2000) and Bertone, Hooper, and Silk (2005) for a review].

A multitude of experimental efforts are currently underway to detect WIMPs, with some claiming hints of detection. There is a three-pronged approach: particle accelerator, indirect detection (astrophysical), and direct detection experiments. The focus of this Colloquium is the third option—direct detection experiments. This field began 30 years ago with the work of Drukier and Stodolsky (1984), who proposed searching for weakly interacting particles (with a focus on neutrinos) by observing the nuclear recoil caused by their weak interactions with nuclei in detectors. Then, Goodman and Witten (1985) made the important point that this approach could be used to search not just for neutrinos but also for WIMPs, again via their weak interactions with detectors. Soon after, Drukier, Freese, and Spergel (1986) extended this work by taking into account the halo distribution of WIMPs in the Milky Way, as well as proposing the annual modulation that is the subject of this Colloquium.

The basic goal of direct detection experiments is to measure the energy deposited when WIMPs interact with nuclei in a detector, causing those nuclei to recoil. The experiments, which are typically located far underground to reduce background contamination, are sensitive to WIMPs that stream through the Earth and interact with nuclei in the detector target. The recoiling nucleus can deposit energy in the form of ionization, heat, and/or light that is subsequently detected. In the mid 1980s, the development of ultrapure germanium detectors provided the first limits on WIMPs (Ahlen *et al.*, 1987). Since then, numerous collaborations worldwide have been searching for these particles, including ANAIS (Amare *et al.*, 2011), ArDM (Marchionni *et al.*, 2011), CDEX/TEXONO (Wong and Lin, 2010), CDMS (Akerib *et al.*, 2005; Ahmed *et al.*, 2010, 2011, 2012), CoGeNT (Aalseth *et al.*, 2011a, 2011b, 2013), COUPP (Behnke *et al.*, 2012), CRESST (Angloher *et al.*, 2012), DAMA/NaI (Bernabei *et al.*, 2003), DAMA/LIBRA (Bernabei *et al.*, 2008, 2010), DEAP/CLEAN (Kos, 2010), DM-Ice (Cherwinka *et al.*, 2012), DRIFT (Alner *et al.*, 2005; Daw *et al.*, 2012), EDELWEISS (Sanglard *et al.*, 2005; Armengaud *et al.*, 2011, 2012), EURECA (Kraus *et al.*, 2011), KIMS (Kim *et al.*, 2012), LUX (Hall *et al.*, 2010), NAIAD (Alner *et al.*, 2005), PandaX (Gong *et al.*, 2013), PICASSO (Barnabe-Heider *et al.*, 2005; Archambault *et al.*, 2012), ROSEBUD (Coron *et al.*, 2011), SIMPLE (Felizardo *et al.*, 2012), TEXONO (Lin *et al.*, 2009), WArP (Acciarri *et al.*, 2011), XENON10 (Angle *et al.*, 2008, 2011; Aprile *et al.*, 2011b), XENON100 (Aprile *et al.*, 2012b, 2012c), XENON1T (Aprile, 2012a), XMASS (Moriyama, 2011), ZEPLIN (Akimov *et al.*, 2007, 2012), and many others.

The count rate in direct detection experiments experiences an annual modulation (Drukier, Freese, and Spergel, 1986; Freese, Frieman, and Gould, 1988) due to the motion of the Earth around the Sun (see Fig. 1). Because the relative velocity of the detector with respect to the WIMPs depends

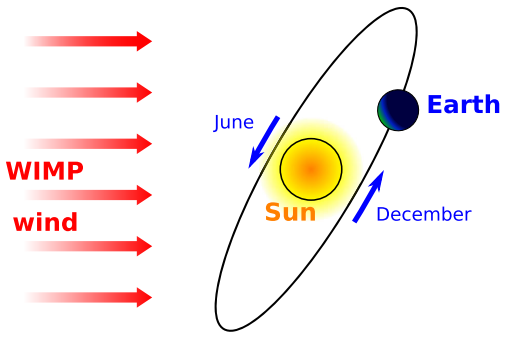

FIG. 1 (color online). A simplified view of the WIMP velocities as seen from the Sun and Earth. Because of the rotation of the galactic disk (containing the Sun) through the essentially nonrotating dark matter halo, the Solar System experiences an effective "WIMP wind." From the perspective of the Earth, the wind changes throughout the year due to the Earth's orbital motion: the wind is at maximum speed around the beginning of June, when the Earth is moving fastest in the direction of the disk rotation, and at a minimum speed around the beginning of December, when the Earth is moving fastest in the direction opposite to the disk rotation. The Earth's orbit is inclined at ~60° relative to the plane of the disk.

on the time of year, the count rate exhibits in most cases a sinusoidal dependence with time. For the simplest assumptions about the dark matter distribution in the halo, the flux is maximal in June and minimal in December. Annual modulation is a powerful signature for dark matter because most background signals, e.g., from radioactivity in the surroundings, are not expected to exhibit this kind of time dependence. The details concerning the recoil energy and modulation spectra depend on the specifics of both the particle physics model and the distribution of WIMPs in the Galaxy. We discuss these possibilities in this Colloquium.

For more than a decade, the DAMA experiment (Bernabei *et al.*, 2008) has been claiming detection of an annual modulation. The experiment, which consists of NaI crystals, is situated in the Gran Sasso Tunnel under the Apennine Mountains near Rome. By now, the amount of data collected is enormous and the statistical significance of the result is undeniable. The DAMA annual modulation is currently reported as almost a 9σ effect (Bernabei *et al.*, 2010) and is consistent with an ~80 or 10 GeV (Bottino *et al.*, 2003, 2004; Gondolo and Gelmini, 2005; Petriello and Zurek, 2008; Chang, Pierce, and Weiner, 2009; Savage *et al.*, 2009b) WIMP elastically scattering predominantly off of iodine or sodium, respectively. Many other direct detection experiments have presented null results that are in clear conflict with the high-mass window. The viability of the 10 GeV WIMP remains a controversial issue because it is not clearly compatible nor clearly incompatible with other null experiments once various detector systematics are taken into account. Recently, the CoGeNT experiment reported a 2.8σ evidence for an annual modulation (Aalseth *et al.*, 2011b) and a third experiment, CRESST-II, has also announced anomalous results (Angloher *et al.*, 2012). Whether DAMA, CoGeNT, and CRESST are consistent in the low-mass window is still debated (Fox *et al.*, 2012; Kelso, Hooper, and Buckley, 2012). Yet CDMS sees no annual modulation (Ahmed *et al.*, 2012), and both CDMS (Ahmed *et al.*, 2010, 2011) and XENON (Angle *et al.*, 2011; Aprile *et al.*, 2012b) find null results that appear to be in conflict with the three experiments that report anomalies.

The current experimental situation in direct detection searches is exciting. Understanding the anomalies and the role that different experiments play in validating them is of crucial importance in moving forward in the search for dark matter. In this Colloquium, we seek to provide the reader with the basic theoretical tools necessary to understand a potential dark matter signature at a direct detection experiment, focusing on the annual modulation of the signal. We begin in Sec. II by reviewing the basics of direct detection techniques for WIMPs, describing the particle physics in Sec. II.A and the astrophysics in Sec. II.B. We describe the standard halo model (SHM) as well as modifications due to substructures. In Sec. III, we examine the behavior of the annual modulation signals for both the SHM and substructures. Although this is primarily a theoretical review, we turn to the experimental status in Sec. IV, briefly reviewing the current anomalies and null results. We conclude in Sec. V. The Appendixes discuss quantities required for understanding results of direct detection experiments. Appendix A describes the quenching factor, and Appendix B presents analytical results for the mean inverse speed for commonly used WIMP velocity distributions, a quantity necessary for a computation of expected count rates in detectors.

II. DARK MATTER DETECTION

Direct detection experiments aim to observe the recoil of a nucleus in a collision with a dark matter particle (Goodman and Witten, 1985). After an elastic collision with a WIMP χ of mass m_χ, a nucleus of mass M recoils with energy $E_{\rm nr} = (\mu^2 v^2/M)(1-\cos\theta)$, where $\mu \equiv m_\chi M/(m_\chi + M)$ is the reduced mass of the WIMP-nucleus system, v is the speed of the WIMP relative to the nucleus, and θ is the scattering angle in the center of mass frame. The differential recoil rate per unit detector mass is

$$\frac{dR}{dE_{\rm nr}} = \frac{n_\chi}{M}\left\langle v\frac{d\sigma}{d}E_{\rm nr}\right\rangle = \frac{2\rho_\chi}{m_\chi}\int d^3v\, v f(\mathbf{v},t)\frac{d\sigma}{dq^2}(q^2,v), \tag{2}$$

where $n_\chi = \rho_\chi/m_\chi$ is the number density of WIMPs, with ρ_χ the local dark matter mass density; $f(\mathbf{v},t)$ is the time-dependent WIMP velocity distribution; and $(d\sigma/dq^2)(q^2,v)$ is the velocity-dependent differential cross section, with $q^2 = 2ME_{\rm nr}$ the momentum exchange in the scatter. The differential rate is typically given in units of cpd kg^{-1} keV^{-1}, where cpd is counts per day. Using the form of the differential cross section for the most commonly assumed couplings, to be discussed below,

$$\frac{dR}{dE_{\rm nr}} = \frac{1}{2m_\chi\mu^2}\sigma(q)\rho_\chi\eta(v_{\rm min}(E_{\rm nr}),t), \tag{3}$$

where $\sigma(q)$ is an effective scattering cross section and

$$\eta(v_{\rm min},t) = \int_{v>v_{\rm min}} d^3v\frac{f(\mathbf{v},t)}{v} \tag{4}$$

is the mean inverse speed, with

$$v_{\rm min} = \begin{cases}\sqrt{\frac{ME_{\rm nr}}{2\mu^2}} & \text{(elastic)},\\ \frac{1}{\sqrt{2ME_{\rm nr}}}\left(\frac{ME_{\rm nr}}{\mu}+\delta\right) & \text{(inelastic)}\end{cases} \tag{5}$$

the minimum WIMP velocity that can result in a recoil energy $E_{\rm nr}$. Here δ is the mass splitting between the lightest and next-to-lightest states in the spectrum in the case of an inelastic scattering interaction[1]; we consider only the elastic scattering case for the remainder of this Colloquium. The benefit of writing the recoil spectrum in the form of Eq. (3) is that the particle physics and astrophysics separate into two

[1]Inelastic scattering with $\delta \simeq \mathcal{O}(100\text{ keV})$ was first invoked to reconcile the DAMA anomaly with the CDMS limits (Tucker-Smith and Weiner, 2001). Although this explanation has since been ruled out by XENON100 for conventional couplings (Aprile *et al.*, 2011a), alternate formulations remain viable as a means of reconciling the experimental results [see, e.g., Chang, Weiner, and Yavin (2010)]. More generally, inelastic scattering (for arbitrary δ) remains an interesting possibility for direct detection experiments, yielding distinct recoil spectra.

factors $\sigma(q)$ and $\rho_\chi \eta(v_{\min}, t)$, respectively.[2] We discuss each of these factors in Sec. II.A and II.B. More detailed reviews of the dark matter scattering process and direct detection can be found in Primack, Seckel, and Sadoulet (1988), Smith and Lewin (1990), Jungman, Kamionkowski, and Griest (1996), Lewin and Smith (1996), and Bertone, Hooper, and Silk (2005).

A. Particle physics: Cross section

For a SUSY neutralino and many other WIMP candidates, the dominant WIMP-quark couplings in direct detection experiments are the scalar and axial-vector couplings, which, respectively, give rise to spin-independent (SI) and spin-dependent (SD) cross sections (Jungman, Kamionkowski, and Griest, 1996). In both cases,

$$\frac{d\sigma}{dq^2}(q^2, v) = \frac{\sigma_0}{4\mu^2 v^2} F^2(q)\Theta(q_{\max} - q) \tag{6}$$

to leading order [see, e.g., Cirigliano, Graesser, and Ovanesyan (2012) for how higher-order corrections can modify this form]. Here Θ is the Heaviside step function, $q_{\max} = 2\mu v$ is the maximum momentum transfer in a collision at a relative velocity v, and the requirement $q < q_{\max}$ gives rise to the lower limit $v > v_{\min}$ in the integral for η in Eq. (4). In Eq. (6), σ_0 is the scattering cross section in the zero-momentum-transfer limit (we use $\sigma_{\rm SI}$ and $\sigma_{\rm SD}$ to represent this term in the SI and SD cases, respectively) and $F^2(q)$ is a form factor to account for the finite size of the nucleus. The WIMP coherently scatters off the entire nucleus when the momentum transfer is small, giving $F^2(q) \to 1$. However, as the de Broglie wavelength of the momentum transfer becomes comparable to the size of the nucleus, the WIMP becomes sensitive to the spatial structure of the nucleus and $F^2(q) < 1$, with $F^2(q) \ll 1$ at higher momentum transfers. It is traditional to define a form-factor corrected cross section

$$\sigma(q) \equiv \sigma_0 F^2(q), \tag{7}$$

as was used in Eq. (3). We note that this is an *effective* cross section, whereas the *actual* scattering cross section is given by $\int dq^2 (d\sigma/dq^2)(q^2, v)$ for a given relative velocity v.

The total WIMP-nucleus scattering rate is then the sum over both the SI and SD contributions, each with its own value of the form factor. We describe these two cross sections below and then briefly discuss more general operators.

1. Spin-independent cross section

The SI WIMP-nucleus interaction, which occurs through operators such as $(\bar\chi\chi)(\bar q q)$, has the cross section

$$\sigma_{\rm SI} = \frac{4}{\pi}\mu^2[Zf_p + (A - Z)f_n]^2, \tag{8}$$

where Z and $A - Z$ are the number of protons and neutrons in the nucleus, respectively, and f_p (f_n) is the effective coupling to the proton (neutron). For neutralinos and most other WIMP candidates with a SI interaction arising through scalar couplings, $f_n \simeq f_p$ and the SI scattering cross sections of WIMPs with protons and neutrons are roughly comparable, $\sigma_{n,\rm SI} \approx \sigma_{p,\rm SI}$. For identical couplings ($f_n = f_p$), the SI cross section can be written as

$$\sigma_{\rm SI} = \frac{\mu^2}{\mu_p^2} A^2 \sigma_{p,\rm SI}, \tag{9}$$

where μ_p is the WIMP-proton reduced mass. As neutralinos are the currently favored WIMP candidate, this assumption is widely made throughout the direct detection literature. Although typically $f_n \simeq f_p$, models can be constructed that violate this condition [e.g., isospin-violating dark matter (Feng *et al.*, 2011)]. We assume identical SI couplings for the rest of this Colloquium.

The SI cross section grows rapidly with nuclear mass. The explicit A^2 factor in Eq. (9) arises from the fact that the contribution to the total SI cross section of a nucleus is a coherent sum over the individual protons and neutrons within. In addition, for WIMPs that are much heavier than the nucleus, $\mu^2/\mu_p^2 \approx A^2$, so the cross section scales as $\sim A^4$. However, the form-factor suppression becomes more significant as the size of the nucleus increases, so the scattering rate does not scale as $\sim A^4$ for heavy nuclei, although it still rises rapidly with A. As a result, direct detection experiments often use heavy nuclei to increase their sensitivity to WIMP scattering.

The SI form factor is essentially a Fourier transform of the mass distribution of the nucleus. A reasonably accurate approximation is the Helm form factor (Helm, 1956; Lewin and Smith, 1996):

$$F(q) = 3e^{-q^2 s^2/2}\frac{\sin(qr_n) - qr_n\cos(qr_n)}{(qr_n)^3}, \tag{10}$$

where $s \simeq 0.9$ fm and $r_n^2 = c^2 + \frac{7}{3}\pi^2 a^2 - 5s^2$ is an effective nuclear radius with $a \simeq 0.52$ fm and $c \simeq 1.23A^{1/3} - 0.60$ fm. Further details on SI form factors can be found in Lewin and Smith (1996) and Duda, Kemper, and Gondolo (2007).

2. Spin-dependent cross section

SD scattering is due to the interaction of a WIMP with the spin of the nucleus through operators such as $(\bar\chi\gamma_\mu\gamma_5\chi) \times (\bar q\gamma^\mu\gamma_5 q)$ and takes place only in those detector isotopes with an unpaired proton and/or unpaired neutron. The SD WIMP-nucleus cross section is

$$\sigma_{\rm SD} = \frac{32\mu^2}{\pi} G_F^2 J(J+1)\Lambda^2, \tag{11}$$

where G_F is the Fermi constant, J is the spin of the nucleus,

$$\Lambda \equiv \frac{1}{J}(a_p\langle S_p\rangle + a_n\langle S_n\rangle), \tag{12}$$

with $\langle S_p\rangle$ and $\langle S_n\rangle$ the average spin contributions from the proton and neutron groups, respectively, and a_p (a_n) the effective couplings to the proton (neutron). Unlike the SI

[2]The ability to separate the particle physics and astrophysics terms as shown requires that the differential scattering cross section $d\sigma/dq^2$ be of the form as in Eq. (6). While this form is expected for the most common types of interactions studied, there are other interactions for which the particle physics and astrophysics cannot be separated as described.

case, the two SD couplings a_n and a_p may differ substantially (although they are often of similar order of magnitude), so that a simplification comparable to Eq. (9) for SI scattering is not made in the SD case. Because of the uncertain theoretical relation between the two couplings and following from the fact that one of $\langle S_p \rangle$ or $\langle S_n \rangle$ is often much smaller than the other, experiments typically only significantly constrain one of the two SD cross sections $\sigma_{p,\mathrm{SD}}$ or $\sigma_{n,\mathrm{SD}}$, but not both.

SD scattering is often of lesser significance than SI scattering in direct detection experiments for two main reasons. First, SI scattering has a coherence factor A^2 that the SD scattering is missing. In fact, the spin factors J, $\langle S_p \rangle$, and $\langle S_n \rangle$ are either zero or $\mathcal{O}(1)$, so the SD cross section does not grow as rapidly with nucleus size as the SI cross section does. Thus, whereas $\sigma_{\mathrm{SI}} \propto A^4$ for heavy WIMPs, $\sigma_{\mathrm{SD}} \propto A^2$ (note that this remaining A^2 factor arises from $\mu^2/\mu_p^2 \approx A^2$). Second, spin-zero isotopes do not contribute to SD scattering, so the SD scattering is reduced in elements where non-zero-spin nuclei represent only a small fraction of the naturally occurring isotopes within a detector's target mass. We note that SD couplings may often be larger than SI couplings; e.g., for an MSSM neutralino, it is often the case that $\sigma_{p,\mathrm{SD}}/\sigma_{p,\mathrm{SI}} \sim \mathcal{O}(10^2$–$10^4)$. However, even with this ratio of couplings, SI scattering is still expected to dominate for the heavy elements used in most detectors for the two reasons described above.

The SD form factor depends on the spin structure of a nucleus and is thus different between individual elements. Form factors for many isotopes of interest to direct detection experiments, as well as estimates of the spin factors $\langle S_p \rangle$ and $\langle S_n \rangle$, can be found in Bednyakov and Simkovic (2005, 2006).

3. General operators

While scalar and axial-vector couplings are the dominant interactions for many WIMP candidates, such as neutralinos, they are by no means the only allowed couplings. In general, dark matter-nucleon interactions can be described by a nonrelativistic effective theory as detailed by Fan, Reece, and Wang (2010) and Fitzpatrick *et al.* (2013). The effective theory approach is useful for highlighting the variety of operator interactions that can exist and their potentially unique direct detection signatures.

Generic operators can give rise to additional factors of the velocity and/or momentum in Eq. (6). Because of the small velocities ($v \sim 10^{-3}c$) and momenta transfers, these interactions are expected to be suppressed relative to the scalar and axial-vector cases and are thus often ignored. However, in models where the scalar and axial-vector couplings are forbidden or suppressed themselves, these new types of interactions can become important.

Consider momentum-dependent (MD) interactions. For certain classes of theories (Masso, Mohanty, and Rao, 2009; Feldstein, Fitzpatrick, and Katz, 2010; Alves *et al.*, 2010; An *et al.*, 2010; Chang, Pierce, and Weiner, 2010), the dominant interactions yield a scattering rate of the form

$$\frac{dR_i^{\mathrm{MD}}}{dE_{\mathrm{nr}}} = \left(\frac{q^2}{q_0^2}\right)^n \frac{dR_i}{dE_{\mathrm{nr}}}, \tag{13}$$

where q_0 is an arbitrary mass scale and $i = \mathrm{SI}, \mathrm{SD}$ denotes whether the rate is independent of nuclear spin or not; dR_i/dE_{nr} is the conventional SI or SD scattering rate described previously. For the most commonly studied operators, $(\bar{\chi}\chi)(\bar{q}q)$ and $(\bar{\chi}\gamma_\mu\gamma_5\chi)(\bar{q}\gamma^\mu\gamma_5 q)$, $n = 0$ and $i = \mathrm{SI}, \mathrm{SD}$, respectively. Generalizations to these scenarios include the operator $(\bar{\chi}\gamma_5\chi)(\bar{q}q)$, which yields an exponent $n = 1$ and a rate that is not dependent on nuclear spin. In contrast, $(\bar{\chi}\gamma_5\chi)(\bar{q}\gamma_5 q)$ has $n = 2$ and $i = \mathrm{SD}$. The momentum dependence in the rate has an important effect on the recoil spectrum, suppressing scattering at low energies. This leads to a peaked recoil spectrum and potentially more high-energy events than would be expected for the case of standard elastic scattering with no momentum dependence, where the rate falls off exponentially.

B. Astrophysics: Dark matter distribution

The velocity distribution $f(\mathbf{v})$ of dark matter particles in the galactic halo affects the signal in dark matter detectors. Here we discuss the velocities of the dark matter components of the halo. The dominant contribution is a smooth virialized component, discussed in Sec. II.B.1. The formation of the Milky Way via merger events leads to significant structure in both the spatial and velocity distributions of the dark matter halo, including dark matter streams and tidal debris, as discussed in Sec. II.B.2.

Velocity distributions are frequently given in a frame other than the laboratory frame to simplify their analytical form. In this Colloquium, we define $\tilde{f}(\mathbf{v})$ as the distribution in the rest frame of the dark matter population (i.e., the frame in which the bulk motion of the dark matter particles is zero); in the case of the (essentially) nonrotating smooth halo background that frame is the galactic rest frame. The laboratory frame distribution is obtained through a Galilean transformation as described in Sec. III. More details of several commonly used distributions, including analytical forms for the mean inverse speed η, can be found in Appendix B.

1. Smooth halo component

The dark matter halo in the local neighborhood is most likely dominated by a smooth and well-mixed (virialized) component with an average density $\rho_\chi \approx 0.4\ \mathrm{GeV/cm^3}$.[3] The simplest model for this smooth component is often taken to be the SHM (Drukier, Freese, and Spergel, 1986; Freese, Frieman, and Gould, 1988), an isothermal sphere with an isotropic, Maxwellian velocity distribution and rms velocity dispersion σ_v. The SHM is written as

[3]Estimates for the local density of the smooth dark matter component are model dependent and vary in the literature by as much as a factor of 2 (Caldwell and Ostriker, 1981; Catena and Ullio, 2010; Pato *et al.*, 2010; Salucci *et al.*, 2010; Weber and de Boer, 2010; Bovy and Tremaine, 2012). Historically, $0.3\ \mathrm{GeV/cm^3}$ has often been assumed when making comparisons between direct detection results. While this density is by no means ruled out by current observations, recent estimates tend to suggest a value closer to $0.4\ \mathrm{GeV/cm^3}$. Both values of the local density can be found in recent direct detection literature.

$$\tilde{f}(\mathbf{v}) = \begin{cases} \frac{1}{N_{\rm esc}}\left(\frac{3}{2\pi\sigma_v^2}\right)^{3/2} e^{-3\mathbf{v}^2/2\sigma_v^2}, & \text{for } |\mathbf{v}| < v_{\rm esc}, \\ 0, & \text{otherwise.} \end{cases} \tag{14}$$

Here

$$N_{\rm esc} = \mathrm{erf}(z) - \frac{2}{\sqrt{\pi}} z e^{-z^2}, \tag{15}$$

with $z \equiv v_{\rm esc}/v_0$, is a normalization factor and

$$v_0 = \sqrt{2/3}\sigma_v \tag{16}$$

is the most probable speed, with an approximate value of 235 km/s (Kerr and Lynden-Bell, 1986; Bovy, Hogg, and Rix, 2009; McMillan and Binney, 2009; Reid *et al.*, 2009) (see Sec. III for further discussion). The Maxwellian distribution is truncated at the escape velocity $v_{\rm esc}$ to account for the fact that WIMPs with sufficiently high velocities escape the Galaxy's potential well and, thus, the high-velocity tail of the distribution is depleted. The dark matter escape velocity in the Milky Way is estimated from that of high-velocity stars. The Radial Velocity Experiment (RAVE) survey finds that the 90% confidence range is 498–608 km/s (Smith *et al.*, 2007). Figure 2 shows the SHM speed distribution in the laboratory (Earth) frame, after accounting for the motion of the solar system relative to the galactic rest frame, as well as the mean inverse speed η.

The sharp cutoff at the escape speed in Eq. (14) is not physical. To smoothen the transition near the escape speed, one may use the (still *ad hoc*) distribution:

$$\tilde{f}(\mathbf{v}) = \begin{cases} \frac{1}{N_{\rm esc}}\left(\frac{3}{2\pi\sigma_v^2}\right)^{3/2}[e^{-3\mathbf{v}^2/2\sigma_v^2} - e^{-3v_{\rm esc}^2/2\sigma_v^2}], & \text{for } |\mathbf{v}| < v_{\rm esc}, \\ 0, & \text{otherwise,} \end{cases} \tag{17}$$

where

$$N_{\rm esc} = \mathrm{erf}(z) - \frac{2}{\sqrt{\pi}} z\left(1 + \frac{2}{3}z^2\right) e^{-z^2}. \tag{18}$$

In another approach, Chaudhury, Bhattacharjee, and Cowsik (2010) used King models to obtain the velocity distribution, handling the finite size and mass of the Galaxy in a more self-consistent manner. In these models, the probability distribution can reach zero at a lower velocity than the escape velocity; essentially, the highest *bound* velocities are unpopulated. In general, because of the large uncertainty in modeling the tail of the velocity distribution, one should approach any result that depends sensitively on high-velocity predictions with caution.

For the conventional SI and SD elastic scattering, the recoil spectrum falls off exponentially in the galactic rest frame for the SHM (neglecting form factors), due to the exponential drop-off with velocity in Eq. (14). Even when form factors and the motion of the Earth through the halo are accounted for, the spectrum is still approximately exponential in the laboratory frame:

$$\frac{dR}{dE_{\rm nr}} \sim e^{-E_{\rm nr}/E_0}, \tag{19}$$

where E_0 is some effective scale that is $\mathcal{O}(10\ \mathrm{keV})$ for typical WIMP and nuclear target masses, so that the largest contribution to the rate in detectors is at low recoil energies. For momentum-dependent interaction operators or inelastic scattering, the rate may instead peak at higher values of recoil energy.

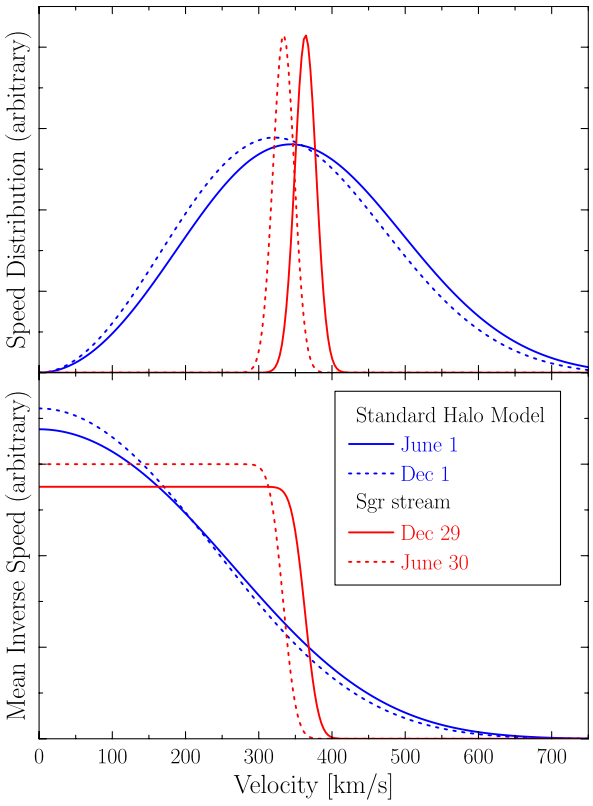

FIG. 2 (color online). Comparison of the standard halo model (SHM) and an example stream, representative of the smooth background halo and a cold flow, respectively. The stream, modeled after the Sagittarius (Sgr) stream, is roughly orthogonal to the galactic plane with speed ~350 km/s relative to the Sun. Upper panel: The speed distribution [one dimensional $f(v)$ in the frame of the Earth] for both components. Lower panel: The differential signal in a detector is directly proportional to the mean inverse speed $\eta(v_{\rm min})$. Here the x axis is $v_{\rm min}$, the lower limit of the integration in Eq. (4). The approximately exponential SHM and steplike stream η's are each shown at two periods of the year, corresponding to the times of year at which η is minimized and maximized; note these times are different for the two components.

The isotropic, Maxwellian velocity distribution of Eq. (14), intended to describe a class of smooth spherical halo models, is only a first approximation of the local halo profile. As reviewed by Green (2012), oblate, prolate, or triaxial halos would be expected to have an anisotropic velocity distribution, which may be approximated as

$$\tilde{f}(\mathbf{v}) \propto \exp\left(-\frac{v_1^2}{2\sigma_1^2} - \frac{v_2^2}{2\sigma_2^2} - \frac{v_3^2}{2\sigma_3^2}\right), \tag{20}$$

where v_i are the WIMP velocities along three perpendicular directions with dispersions σ_i. In general, changes to the halo shape from anisotropy result in $\mathcal{O}(10\%)$ changes in the annual modulation signal (Green, 2001, 2010), although a more exact statement depends on the dark matter properties and the detector threshold.

High-resolution cosmological N-body simulations provide evidence that a Maxwellian distribution does not fully capture the velocity distribution of the smooth halo component, particularly along the high-velocity tail, which is important for detection of low-mass WIMPs as detectors are sensitive only to the highest velocity WIMPs in this case. Kuhlen *et al.* (2010) determined the velocity distribution from two of the highest resolution numerical simulations of galactic dark matter structure [Via Lactea II (Diemand, Kuhlen, and Madau, 2007; Diemand *et al.*, 2008) and GHALO (Stadel *et al.*, 2008)]. They found more low speed particles than in a Maxwellian case and a distribution with a peak that is flatter in shape. Alternatively, analytic fits for producing better agreement with numerical results at the high-speed tail have been obtained (Lisanti *et al.*, 2011; Mao *et al.*, 2013).

Another issue is that most simulations contain only dark matter particles; simulating baryonic physics is extremely difficult, but important given that baryons dominate in the inner regions of the Milky Way. Gas cooling changes halo shapes from prolate triaxial to more spherical when baryons are added (Dubinski and Carlberg, 1991; Kazantzidis *et al.*, 2004; Debattista *et al.*, 2008; Valluri *et al.*, 2009; Zemp *et al.*, 2012), with velocity distributions that are expected to deviate less from the standard Maxwellian than those found in dark matter-only simulations. Purcell, Zentner, and Wang (2012) studied predictions for dark matter experiments within the context of an isolated numerical model of a Milky Way-like system designed to reproduce the basic properties of the Galaxy by including an equilibrated galactic stellar disk and the associated Sagittarius galaxy impact, in addition to dark matter. The resulting dark matter velocity distribution still exhibits deviations from Maxwellian and the calculated recoil spectrum has an increased number of scattering events at large energies.

Using cosmological simulations, Read *et al.* (2008a, 2008b) and Purcell, Bullock, and Kaplinghat (2009) identified the possibility of a disklike dark matter component (“dark disk”) that forms from satellite merger events. Ling *et al.* (2010) performed a high-resolution cosmological N-body simulation with baryons. They studied a Milky Way sized object at redshift $z = 0$ that included gas, stars, and dark matter to characterize the corotating dark disk, which could play an important role in direct detection experiments (Bruch *et al.*, 2009). Equilibrated self-gravitating collisionless structures have been shown to exhibit Tsallis distributions (Tsallis, 1988; Lima, Silva, and Plastino, 2001; Hansen *et al.*, 2005, 2006):

$$\tilde{f}(\mathbf{v}) = \frac{1}{N(v_0, q)}\left[1 - (1-q)\frac{\mathbf{v}^2}{v_0^2}\right]^{q/(1-q)}, \tag{21}$$

where $N(v_0, q)$ is a normalization constant and the Maxwell-Botzmann distribution is recovered by taking the limit $q \to 1$. For a spherical shell at the same radial distance as the Sun in the Ling *et al.* simulation, the velocity distribution is best fit by a Tsallis distribution with $v_0 = 267.2$ km/s and $q = 0.773$. In an analysis of the dark matter and stars in the cosmological hydro simulation of Stinson *et al.* (2010), Valluri *et al.* (2013) also found higher tangential motion in dark matter particles close to the disk plane than away from it, consistent with a dark disk.

2. Unvirialized structure of halo

The Milky Way halo forms through the merging of smaller dark matter subhalos. These merging events can lead to significant structure in both the spatial and velocity distribution of the dark matter halo. High-resolution cosmological dark matter simulations, such as Via Lactea (Diemand, Kuhlen, and Madau, 2007; Diemand *et al.*, 2008), GHALO (Stadel *et al.*, 2008), and Aquarius (Springel *et al.*, 2008), find residual substructure from the merging process that includes dark matter clumps, cold streams, and debris flows. The dark matter affiliated with any of these substructures located in the solar neighborhood affects count rates and spectra as well as the phase and amplitude of the annual modulation in experiments (Gelmini and Gondolo, 2001; Stiff, Widrow, and Frieman, 2001; Freese *et al.*, 2004; Freese, Gondolo, and Newberg, 2005; Savage, Freese, and Gondolo, 2006; Kuhlen *et al.*, 2010; Purcell, Zentner, and Wang, 2012; Alves, Lisanti, and Wacker, 2010; Kuhlen, Lisanti, and Spergel, 2012).

An example of a spatially localized substructure is a dense clump or subhalo of dark matter. If the Earth is sitting in such a clump, the local dark matter density would be larger than currently expected, increasing scattering rates in experiments. According to numerical simulations, however, local density variations due to the clumpiness of the dark matter halo are unlikely to significantly affect the direct detection scattering rate. Based on the Aquarius Project, Vogelsberger *et al.* (2009) reported that the dark matter density at the Sun's location differs by less than 15% from the average at more than 99.9% confidence and estimates a probability of 10^{-4} for the Sun being located in a bound subhalo of any mass. The possibility that the Earth may reside in a local underdensity due to unvirialized subhalos throughout the Galaxy should also be taken into account when interpreting direct detection null results; Kamionkowski and Koushiappas (2008) predicted a positively skewed density distribution with local densities as low as one-tenth the mean value, but probably not much less than half.

In addition to structure in configuration space, the dark matter halo can also exhibit velocity substructure in the form of debris flows or cold tidal streams. Debris flows are an example of a spatially homogenous velocity substructure that consists of the overlapping shells, sheets, and plumes formed from the tidal debris of the (sum total of) subhalos falling into the Milky Way (Kuhlen, Lisanti, and Spergel, 2012; Lisanti and Spergel, 2012). Although this dark matter component is spatially uniform, the distribution of its galactocentric speeds is roughly a delta function.[4] In Via Lactea II, more than half of the dark matter near the Sun with (Earth-frame) speeds greater than 450 km/s is debris flow. At higher speeds, debris flow comprises over 80% of the dark matter. As a result, debris flow is particularly important for experiments that probe the high-velocity tail of the dark matter distribution, such as searches for light dark matter or experiments with directional sensitivity.

Tidal streams are another unvirialized component of the halo and also consist of material stripped from infalling

[4]Note the distinction between a delta function in the speed for a debris flow and a delta function in the velocity for a stream (below).

satellites. As the material in the stream has not had the time to spatially mix, the stream has a small velocity dispersion in comparison to that of the virialized halo. A dark matter stream is coherent in velocity space, with

$$\tilde{f}_{\rm str}(\mathbf{v}) = \delta^3(\mathbf{v}) \tag{22}$$

in the limit of zero dispersion. In some cases, particularly when examining the annual modulation signal, it may be important to account for the small but non-negligible dispersion of the stream. In such cases, a Maxwellian velocity distribution[5] can be used, albeit with a much smaller σ_v than that for the SHM. The speed distribution of an example stream in the laboratory frame, as well as the corresponding η, are shown in Fig. 2.

The Sagittarius stream is one of the most stunning examples of a stellar stream in our Galaxy. Sagittarius (Sgr) is a satellite galaxy that is located inside the Milky Way on the opposite side of the Galactic center from the Sun; it is currently being disrupted and absorbed by the Milky Way. The Sloan Digital Sky Survey and the Two Micron All Sky Survey (Majewski *et al.*, 2003; Newberg *et al.*, 2003; Yanny *et al.*, 2003) have traced the stellar component of the tidal stream (Dohm-Palmer *et al.*, 2001; Ibata *et al.*, 2001). Two streams of matter are being tidally pulled away from the main body of the Sgr galaxy and extend outward from it. Whether the Sgr stream passes close enough to the solar neighborhood to affect direct detection experiments remains up for debate. Early data indicated that the leading tail of stellar material ripped from the Sgr galaxy passes only a few kpc from the solar neighborhood (Belokurov *et al.*, 2006; Seabroke *et al.*, 2007), but later studies indicated that the center of the stream's stellar component could be farther away than initial estimates suggested (Fiorentin *et al.*, 2010). Most recently, however, Purcell, Zentner, and Wang (2012) analyzed self-consistent N-body simulations of the Milky Way disk and the ongoing disruption of the Sgr dwarf galaxy and argued that the dark matter part of the Sgr stream may, in fact, impact the Earth. Streams can have a variety of effects on direct detection experiments (Freese *et al.*, 2004; Freese, Gondolo, and Newberg, 2005), as discussed further below.

Alternative models of halo formation, such as the late-infall model (Gunn, Gott, and Richard, 1972; Fillmore and Goldreich, 1984; Bertschinger, 1985) more recently examined by Sikivie and others (Sikivie and Ipser, 1992; Sikivie, Tkachev, and Wang, 1997; Sikivie, 1998, 1999; Tremaine, 1999; Natarajan and Sikivie, 2005; Natarajan, 2011), also predict cold flows of dark matter. In the caustic ring model (Duffy and Sikivie, 2008), the annual modulation is 180° out of phase compared to the usual (isothermal) model. Any such streaming of WIMPs (we henceforth use "stream" to imply any cold flow) will yield a significantly different modulation effect than that due to a smooth halo.

[5]Tidal streams can have much more anisotropic velocity distributions than the smooth halo background, with a larger dispersion along the longitudinal direction than transverse directions (Stiff, Widrow, and Frieman, 2001). Still, the isotropic Maxwellian distribution with an appropriately chosen σ_v can provide a sufficiently good approximation for the purposes of direct detection calculations.

Finally, there may be unbound dark matter of extragalactic origin passing through the Galaxy. If present, these high-speed particles can increase the number of high-energy scattering events in a direct detection experiment (Freese, Gondolo, and Stodolsky, 2001; Baushev, 2013).

III. ANNUAL MODULATION

The velocity distribution in the Earth's frame $f(\mathbf{v}, t)$ changes throughout the year due to the time-varying motion of an observer on Earth. Assuming $\tilde{f}(\mathbf{v})$ is the velocity distribution in the rest frame of the dark matter population, i.e., the frame where the bulk motion is zero, the velocity distribution in the laboratory frame is obtained after a Galilean boost:

$$f(\mathbf{v}, t) = \tilde{f}(\mathbf{v}_{\rm obs}(t) + \mathbf{v}), \tag{23}$$

where

$$\mathbf{v}_{\rm obs}(t) = \mathbf{v}_\odot + \mathbf{V}_\oplus(t) \tag{24}$$

is the motion of the laboratory frame relative to the rest frame of the dark matter, $\mathbf{v}_\odot$ is the motion of the Sun relative to that frame, and $\mathbf{V}_\oplus(t)$ is the velocity of the Earth relative to the Sun. For a nonrotating, smooth background halo component, such as the SHM, $\mathbf{v}_\odot = \mathbf{v}_{\rm LSR} + \mathbf{v}_{\odot,\rm pec}$, where $\mathbf{v}_{\rm LSR} = (0, v_{\rm rot}, 0)$ is the motion of the local standard of rest in galactic coordinates,[6] and $\mathbf{v}_{\odot,\rm pec} = (11, 12, 7)$ km/s is the Sun's peculiar velocity [see, e.g., Mignard (2000) and Schoenrich, Binney, and Dehnen (2009) and references therein]. The canonical value for the disk rotation speed $v_{\rm rot}$ has long been 220 km/s (Kerr and Lynden-Bell, 1986), but more recent estimates tend to place it 5%–15% higher (Bovy, Hogg, and Rix, 2009; McMillan and Binney, 2009; Reid *et al.*, 2009). A value of 235 km/s is more centrally located within current estimates and is more frequently being used as a fiducial value, although 220 km/s remains viable.

The $\mathbf{V}_\oplus(t)$ term in Eq. (24) varies throughout the year as the Earth orbits the Sun, leading to an annual modulation in the velocity distribution and, thus, the recoil rate. Written out in full,

$$\mathbf{V}_\oplus(t) = V_\oplus[\hat{\boldsymbol{\varepsilon}}_1 \cos\omega(t - t_1) + \hat{\boldsymbol{\varepsilon}}_2 \sin\omega(t - t_1)], \tag{25}$$

where $\omega = 2\pi/\text{yr}$, $V_\oplus = 29.8$ km/s is the Earth's orbital speed around the Sun, and $\hat{\boldsymbol{\varepsilon}}_1$ and $\hat{\boldsymbol{\varepsilon}}_2$ are the directions of the Earth's velocity at times t_1 and $t_1 + 0.25$ yr, respectively. Equation (25) neglects the ellipticity of the Earth's orbit, which is small and gives only negligible changes to the velocity expression [see Lewin and Smith (1996) and Green (2003) for more detailed expressions]. In galactic coordinates,

$$\begin{aligned} \hat{\boldsymbol{\varepsilon}}_1 &= (0.9931, 0.1170, -0.010\,32) \quad \text{and} \\ \hat{\boldsymbol{\varepsilon}}_2 &= (-0.0670, 0.4927, -0.8676), \end{aligned} \tag{26}$$

[6]Galactic coordinates are aligned such that $\hat{\mathbf{x}}$ is the direction to the Galactic center, $\hat{\mathbf{y}}$ is the direction of the local disk rotation, and $\hat{\mathbf{z}}$ is orthogonal to the plane of the disk.

where $\hat{\boldsymbol{\varepsilon}}_1$ and $\hat{\boldsymbol{\varepsilon}}_2$ are the directions of the Earth's motion at the spring equinox (21 March, or t_1) and summer solstice (21 June), respectively.

If we define the characteristic time t_0 as the time of year at which $v_{\rm obs}(t)$ is maximized, i.e., the time of year at which Earth is moving fastest with respect to the rest frame of the dark matter, then the magnitude of $v_{\rm obs}(t)$ is

$$v_{\rm obs}(t) \approx v_\odot + bV_\oplus \cos\omega(t - t_0), \tag{27}$$

where $b \equiv \sqrt{b_1^2 + b_2^2}$ for $b_i \equiv \hat{\boldsymbol{\varepsilon}}_i \cdot \hat{\mathbf{v}}_\odot$ is a geometrical factor associated with the direction of $\mathbf{v}_{\rm obs}$ relative to Earth's orbital plane (note $|b| \leq 1$). The approximation is valid when $V_\oplus/v_\odot \ll 1$, as is the case with nearly all halo components.

Once the Galilean transformation of Eq. (23) is performed, $\eta(v_{\rm min}, t)$ is calculated via Eq. (4); see Appendix B for analytical forms of η for several commonly used distributions. Because the modulation rate must have a fixed period of 1 yr,[7] the differential scattering rate can be expanded in a Fourier series:

$$\frac{dR}{dE}(v_{\rm min}, t) = A_0 + \sum_{n=1}^{\infty} A_n \cos n\omega(t - t_0) + \sum_{n=1}^{\infty} B_n \sin n\omega(t - t_0), \tag{28}$$

where the Fourier coefficients A_n and B_n are functions of $v_{\rm min}$ [see Eq. (5)]. If the velocity distribution in the rest frame of the dark matter is isotropic, then $B_n = 0$. This simplification is a direct result of expanding about t_0: although the Fourier expansion could be made about any other (arbitrary) phase, the sum would include both cosine and sine terms. The expansion in terms of only cosines is not surprising as $v_{\rm obs}(t)$ contains only a single cosine term in Eq. (27). This simplification does not apply for anisotropic distributions; however, for nearly all realistic anisotropic distributions $B_n \ll A_n$, and the sine terms in the expansion can still be neglected. As a consequence, the modulation will always be symmetric (or very nearly so) about the characteristic time t_0.

For smooth components of the halo, such that $f(\mathbf{v})$ is slowly varying over $\delta\mathbf{v} \sim V_\oplus$, one further finds that $A_0 \gg A_1 \gg A_{n\geq 2}$, assuming $v_\odot \gg V_\oplus$ as is the case for most components of the halo. This relation further holds for any structure in the halo when $f(\mathbf{v})$ is slowly varying for $|\mathbf{v}| \approx v_{\rm min}$, as is the case for cold flows where $v_{\rm min} \not\approx v_\odot$. Higher-order terms in the Fourier expansion may become important when $f(\mathbf{v})$ exhibits sharp changes in the vicinity of $|\mathbf{v}| \approx v_{\rm min}$, which can happen in the case of a stream.

Except for the special cases described above, the annually modulating recoil rate can be approximated by

$$\frac{dR}{dE}(E, t) \approx S_0(E) + S_m(E)\cos\omega(t - t_0), \tag{29}$$

with $|S_m| \ll S_0$, where S_0 is the time-averaged rate, S_m is referred to as the modulation amplitude (which may, in fact, be negative), $\omega = 2\pi/\text{yr}$, and t_0 is the phase of the modulation.[8] The quantities S_0 and S_m correspond to A_0 and A_1, respectively, in the Fourier expansion of Eq. (28), but the former are the standard notation in the literature when only the constant and first cosine terms of the Fourier expansion are used.

In addition to the time-varying motion of a detector due to the orbit of the Earth about the Sun, there is a time-varying motion due to the rotation of the Earth about its axis, leading to a daily (diurnal) modulation in the recoil rate. This modulation can be determined by repeating the above procedure with the inclusion of this rotational velocity term in Eq. (24). However, the rotational velocity (at most 0.5 km/s, near the equator) is significantly smaller than the orbital velocity (30 km/s), making the daily modulation signal much smaller than the annual modulation signal and, unfortunately, much more difficult to detect (made more difficult by the statistical issues of extracting the modulation from an experimental result, as discussed below). For this reason, the daily modulation in the recoil rate is typically ignored in modulation searches. A related, but different, effect is the daily modulation in the recoil *direction*, a much larger effect that may be observed by directional detectors, briefly discussed in Sec. IV.C.

Detecting the modulation signal in an experiment is made difficult by the fact that the modulation S_m must be extracted from on top of a large constant rate S_0. Here we use a very simple two bin analysis to illustrate the statistical issues in experimentally extracting a modulation amplitude. Suppose an experiment counts events over a one year period, dividing those events into the six month periods centered on t_0 and $t_0 + 0.5$ yr; we use $+$ and $-$ subscripts to refer to these two respective periods. Assuming a modulation of the form given by Eq. (29), these are the periods when the rate is above and below average, respectively. The experimental estimates of the average rate and the modulation amplitude are

$$S_0' \sim \frac{1}{MT\Delta E}(N_+ + N_-) \quad \text{and} \quad S_m' \sim \frac{1}{MT\Delta E}(N_+ - N_-), \tag{31}$$

where $MT\Delta E$ is the exposure of the detector, M is the target mass, $T = 1$ yr is the total exposure time, ΔE is the width of the energy range considered, and $N_\pm$ are the number of events measured in each bin. The uncertainty δS_m in the amplitude can be determined from simple error propagation in terms of the two measurements $N_\pm$:

$$(\delta S_m')^2 = \left(\frac{\partial S_m'}{\partial N_+}\right)^2 (\delta N_+)^2 + \left(\frac{\partial S_m'}{\partial N_-}\right)^2 (\delta N_-)^2 \sim \left(\frac{1}{MT\Delta E}\right)^2 (N_+ + N_-), \tag{32}$$

[7]The density and intrinsic velocity distribution will change as the Solar System moves into, through, and back out of any substructure of finite size, such as a clump, leading to variations in the recoil rate that do not manifest as an annual modulation. However, the time scales involved are typically many orders of magnitude longer than a year and such temporal variations can be neglected.

[8]Experiments may quote the average amplitude over some interval,

$$\bar{S}_m = \frac{1}{E_2 - E_1}\int_{E_1}^{E_2} dE S_m(E). \tag{30}$$

where $\delta N_{\pm} = \sqrt{N_{\pm}}$ are the errors in the counts. The statistical significance of the measured modulation amplitude is

$$\frac{S'_m}{\delta S'_m} \propto \sqrt{\frac{MT\Delta E S'^2_m}{S'_0}} \propto \sqrt{N_T}\frac{S'_m}{S'_0}, \tag{33}$$

where $N_T \equiv N_+ + N_-$ is the total number of events. While this derivation is for a simple two bin analysis of the yearly modulation, the above proportionality relationship holds true for any modulation signal and analysis scheme: a reduction in the modulation amplitude S_m by a factor of 2 requires an increase in the number of detected events N_T (and hence exposure) by a factor of 4 to be detected to the same statistical significance. Thus, to detect the daily modulation signal to the same significance as the annual modulation signal, where the amplitude of the former is $\gtrsim 60$ times smaller than the latter (Earth's surface rotational speed of $\lesssim 0.5$ km/s versus an orbital speed of 30 km/s), requires an increase in exposure by a factor of at least $\mathcal{O}(60^2)$, a daunting task.

In the remainder of this section, we examine the modulation for the SHM and substructure components. Figure 3 summarizes the conclusions we reach. Note that the expected modulation amplitude depends sensitively on the assumed dark matter velocity distribution. In reality, the local dark matter is likely comprised of both a virialized and an unvirialized component, meaning that a signal at a direct detection experiment may be due to several different dark matter components. In this case, a modulation of the form given by Eq. (29) with a fixed phase t_0 may not be a good approximation; the shape of the modulation for the total rate may no longer be sinusoidal in shape and/or the phase may vary with $v_{\min}$. Furthermore, there are cases when Eq. (29) is a bad approximation even for a single halo component; an example is shown below for a stream. We conclude this section with a discussion of what can be learned about the local halo in these more complicated scenarios.

A. Smooth background halo: Isothermal (standard) halo model

We now apply our general discussion of the modulation rate to the example of a simple isothermal sphere (Freese, Frieman, and Gould, 1988). As discussed in Sec. II.B, the SHM is almost certainly not an accurate model for the dark matter velocity distribution in the Milky Way. However, its simple analytic form provides a useful starting point for gaining intuition about the modulation spectrum of the virialized dark matter component.

As shown in Eq. (3), the differential count rate in a detector is directly proportional to the mean inverse speed η; the time dependence of the recoil rate arises entirely through this term. To study the expected time dependence of the signal in the detector, we therefore focus on the time dependence of η; in particular, we investigate the annual modulation of the quantity η as it is the same as that of the dark matter count rate.

For the SHM or any dark matter component with a velocity distribution described by Eq. (14) or (17), the mean inverse speed has an analytical form, presented in Appendix B and in Savage, Freese, and Gondolo (2006) and McCabe (2010). Figure 2 illustrates $\eta(v_{\min})$ for the SHM, taking $v_0 = v_{\rm rot}$ as expected for an isothermal spherical halo.

Figure 2 shows $\eta(v_{\min})$ at $t_0 \simeq$ June 1, the time of year at which the Earth is moving fastest through the SHM, as well as on 1 December, when the Earth is moving slowest; there is a (small) change in η over the year. The corresponding recoil spectra, as a function of recoil energy, are given in schematic form in the first panel of Fig. 3. The amplitude of the modulation,

$$A_1(E) \approx \frac{1}{2}\left[\frac{dR}{dE}(E, \text{June } 1) - \frac{dR}{dE}(E, \text{Dec } 1)\right], \tag{34}$$

is also shown in the figure. Two features of the modulation are apparent for the SHM: (1) the amplitude of the modulation is small relative to the average rate, with an exception to be

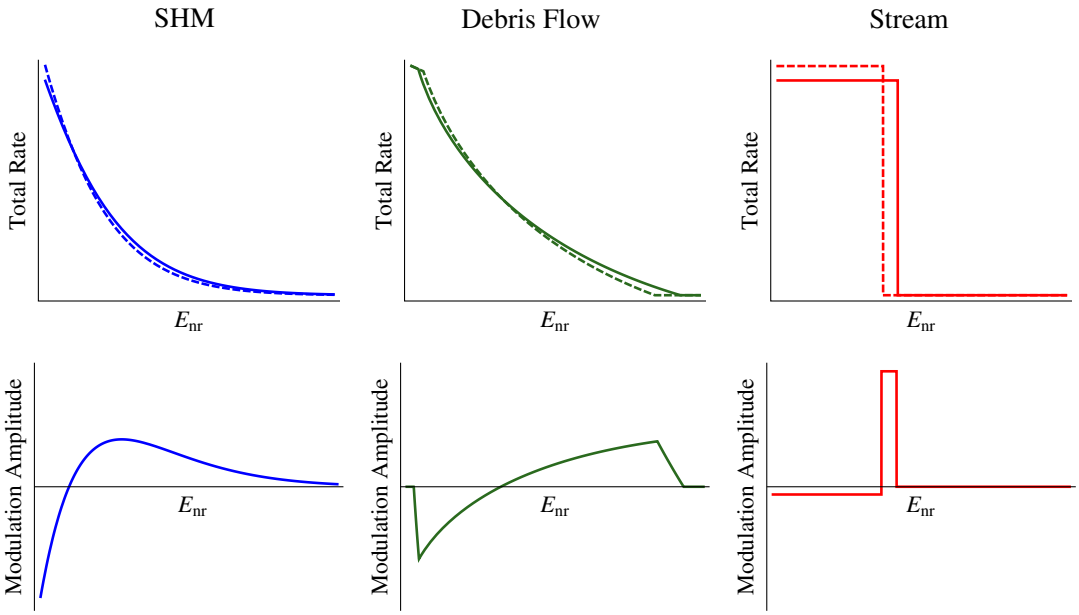

FIG. 3 (color online). Comparison of the shapes of the total rate shown at two periods of the year, corresponding to the times of year at which the rate is minimized and maximized, as well as the modulation amplitude, for three different halo components: SHM (left), debris flow (middle), and stream (right). The normalization between panels is arbitrary.

discussed below, and (2) the amplitude of the modulation changes sign at small $v_{\rm min}$ (low recoil energies). This phase reversal can be used to constrain the WIMP mass.

Figure 4 illustrates the residual time-varying signal for the SHM (dashed curves). The different panels show how the modulation depends on $v_{\rm min}$. In general, the modulation has a sinusoidal shape and is symmetric about t_0; the sinusoidal shape allows for the use of the amplitude approximation given by Eq. (34). For small $v_{\rm min}$ (low recoil energies), the rate is *minimized* at a time t_0, while for large $v_{\rm min}$ (high recoil energies), the rate is *maximized* at t_0.

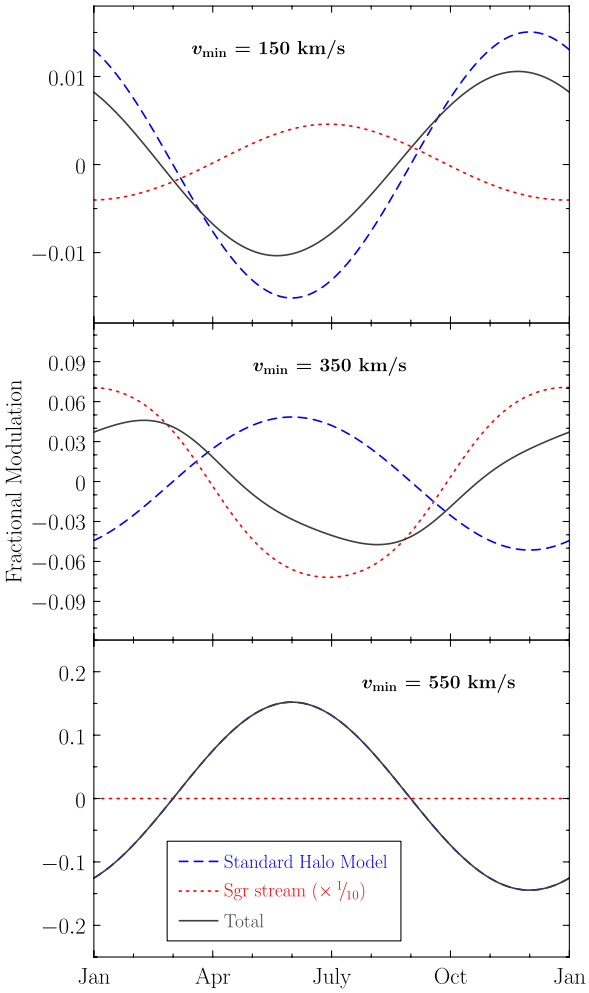

FIG. 4 (color online). The residual rate for the SHM (dashed) and an example stream (dotted) is plotted at several values of $v_{\rm min}$. The stream is modeled after the Sgr stream. Also shown is the total SHM + stream modulation, assuming the local density of the stream is 10% that of the SHM. The residual rates are given relative to the average rate in each case, i.e., curves show the *fractional* modulation, except for the stream, where the relative rate has been divided by 10 for visual clarity as its relative modulation is much larger. The corresponding recoil energy for each $v_{\rm min}$, given by Eq. (5), depends on the WIMP and nuclear target masses; for a WIMP mass of 60 GeV and a germanium target, the $v_{\rm min}$ values of 150, 350, and 550 km/s correspond to recoil energies of 7, 40, and 100 keV, respectively. The phase reversal of the SHM component, which occurs at smaller $v_{\rm min}$, can be seen by comparing the dashed curves in the top two panels. The recoil energy at which this phase reversal takes place can be used to determine the WIMP mass. From Lewis and Freese, 2004.

An important quantity of interest is the *modulation fraction*, defined as the size of the modulation amplitude relative to the average total rate S_m/S_0. For a wide range of $v_{\rm min}$, the modulation fraction is $\mathcal{O}(1\%–10\%)$, as seen in Fig. 4. For $v_{\rm min}$ above ~500 km/s, both S_0 and S_m fall rapidly with $v_{\rm min}$ as scatters come only from WIMPs in the tail of the Maxwellian distribution. In this region, S_0 falls more rapidly, so the modulation fraction grows, going from $\mathcal{O}(10\%)$ to $\mathcal{O}(100\%)$. Because of the low absolute rates at these higher energies, experiments are generally not sensitive to the $v_{\rm min}$ region with high modulation fraction. However, for WIMPs that are much lighter than the nuclear target, large modulation fractions correspond to the recoil energies of interest in detectors, and an order unity modulation can be observed.[9]

As noted previously, the phase reversal of the annual modulation, illustrated in Fig. 4, can be used to determine the WIMP mass (Lewis and Freese, 2004) and is perhaps the best feature of a direct detection signal for doing so. While the phase of the modulation is fixed for a given $v_{\rm min}$, regardless of the WIMP mass, the phase of the modulation for a given recoil energy $E_{\rm nr}$ is not, as the $E_{\rm nr}$ associated with a given $v_{\rm min}$ is dependent on the WIMP mass through Eq. (5). Thus, an experimental determination of the recoil energy at which the phase reverses, which occurs at $v_{\rm min} \approx 210$ km/s for the SHM, can constrain the WIMP mass. For a germanium detector, the SHM phase reversal is expected to occur at recoil energies of 1, 5, and 15 keV for WIMP masses of 10, 25, and 60 GeV, respectively; the modulation spectrum should be readily distinguishable between these cases. As the WIMP gets much heavier than the target nucleus, the recoil spectrum becomes degenerate and the energy of the phase reversal approaches a fixed value (62 keV for germanium); observation of a reversal at this energy allows only a lower limit to be placed on the WIMP mass.[10] We emphasize the fact that detection of this phase reversal could constitute an important signature of a WIMP flux as backgrounds would not give rise to such an effect.

As discussed in Sec. II.B, the SHM may not be an accurate model of the smooth background halo. However, the generic features of the SHM modulation signal discussed here are also features to be expected of any smooth background halo model. In particular, the modulation should be sinusoidal in shape with a phase around the beginning of June, have an

[9]When the size of the variations in the recoil rate throughout the year becomes comparable to the average rate, i.e., the relative modulation amplitude is of order unity, Eq. (34) is no longer a good approximation to the modulation. A significant deviation from a cosinusoidal modulation would be an expected signature for large modulation fractions.

[10]A caveat regarding extracting limits on the WIMP mass from the phase reversal is in order. As illustrated shortly, cold flows (such as streams or caustics) can strongly affect the phase of the modulation. Thus, the phase of the annual modulation constrains the WIMP mass only when the distribution of particle velocities in the solar neighborhood is known. One may, however, use the results of two different experiments to constrain the mass without assuming a form for the velocity distribution (Drees and Shan, 2007, 2008).

$\mathcal{O}(1\%–10\%)$ modulation amplitude (except at high $v_{\min}$), and have a phase reversal (Green, 2001, 2002, 2010). However, all these features can be significantly altered if there is any significant substructure present in the halo, so we turn to substructure next.

B. Halo substructure

Next we consider the modulation spectrum when the dark matter scattering in the detector is dominated by unvirialized components in the halo, such as debris flows or streams. Figure 3 illustrates how the modulated and total rates in these cases can differ drastically from that expected from a smooth halo contribution. For a complete discussion of the modulation spectra for dark matter streams, see Savage, Freese, and Gondolo (2006). A simple analytic approximation for the mean inverse speed of the debris flow is given by Kuhlen, Lisanti, and Spergel (2012), from which it is straightforward to derive the modulated and total rates (see also Appendix B).

Figure 3 emphasizes the fact that substructure components can increase the number of expected scattering events at large recoil energies, in comparison to the smooth halo contribution. This is due to the fact that velocity substructure is most likely to be found near the escape velocity, where the dark matter is predominantly not in equilibrium. In particular, while the modulation amplitude for a smooth halo falls with energy, that for debris flows and streams can peak at large values. Therefore, a larger-than-expected modulation at high recoil energies can be an important indicator for dark matter substructure in the local neighborhood.

As an example of a substructure component, we now consider the case of a dark matter stream more fully. For the case of a dispersionless dark matter stream, the recoil spectrum is proportional to

$$\eta_{\rm str}(v_{\min}, t) = \frac{\theta(v_{\rm obs}(t) - v_{\min})}{v_{\rm obs}(t)}, \tag{35}$$

where θ is the Heaviside function and is flat up to the cutoff energy

$$E_c(t) = \frac{2\mu^2}{M} v_{\rm obs}(t)^2. \tag{36}$$

This characteristic energy is the maximum recoil energy that can be imparted to the nucleus and is obtained as follows: The maximum momentum transferred from a WIMP to a nucleus occurs when the nucleus recoils straight back and is $q_{\max} = 2\mu v_{\rm obs}(t)$. The maximum recoil energy of the nucleus then follows as $E_c(t) = q_{\max}^2/(2M)$. A small, but nonzero velocity dispersion σ_v expected in, e.g., tidal streams can soften the sharp edge of the step-shaped η. The velocity dispersion for the Sagittarius stellar stream, for example, is roughly $\mathcal{O}(20$ km/s) (Dohm-Palmer *et al.*, 2001; Majewski *et al.*, 2003; Yanny *et al.*, 2003; Carlin *et al.*, 2012). The dark matter in a tidal stream can be expected to have a velocity dispersion of a similar magnitude, although how closely it matches the dispersion of the stars remains an open question.

We take as an example a stream with velocity and direction similar to what may be expected if the Sgr stream is accompanied by a broader stream of dark matter that passes near the solar neighborhood (Freese *et al.*, 2004; Freese, Gondolo, and Newberg, 2005; Purcell, Zentner, and Wang, 2012). This is intended as a concrete example of a more general phenomena and will illustrate the basic features of an annual modulation signal in the presence of a stream. The stream in our example is roughly orthogonal to the galactic plane and moves at a speed $\sim$350 km/s relative to the Sun. Its speed distribution and mean inverse speed η are shown in Fig. 2; in the latter case, the steplike spectrum (with a softened edge) is evident. For this stream, $v_{\rm obs}(t)$ is maximal on 29 December and minimal on 30 June.

There are two distinct features of a stream's recoil spectrum that modulate: (1) the height of the step and (2) the location of the step edge. Unlike the SHM, the relative modulation amplitude is fairly uniform at all $v_{\min}$ below the velocity of the stream in the laboratory frame, although, like the SHM, the modulation is small compared to the total rate. This modulation, seen in the top panel of Fig. 4, is sinusoidal and peaks in late December. Above the stream's velocity in the laboratory frame, the signal vanishes because there are no available dark matter particles (lower panel of Fig. 4).

The modulation becomes interesting when the minimum scattering velocity is approximately equal to the stream's velocity in the laboratory frame $v_{\min} \approx v_\odot \approx 350$ km/s. This occurs near the edge of the step in the recoil spectrum. As illustrated in Fig. 3, η changes by a relatively large amount throughout the year for $v_{\min} \approx v_\odot$, leading to a very large modulation. The modulation at the softened edge of the example stream, shown in the middle panel of Fig. 4, has a relative amplitude of nearly 70%, much larger than that for the SHM. Although not apparent in this figure, this is one of the special cases where the higher-order terms of Eq. (28) can become important and the modulation deviates from a sinusoidal shape; see Fig. 7 of Savage, Freese, and Gondolo (2006) for a clearer example. This very large modulation, which occurs over only a narrow range of recoil energies, has a phase reversed from that at lower energies.

The features of the modulation for our example stream are expected of any cold flow (stream). Up to some cutoff energy, the modulation is uniform, relatively small, and sinusoidal. Above the cutoff energy, the modulation, as well as the total rate, is negligible. Over a narrow range of energies about the cutoff energy, the modulation can be very large and possibly nonsinusoidal. However, the phase of the modulation and cutoff energy can vary significantly depending on the direction and speed of the stream. Observation of unexpected phases in the modulation and/or a narrow energy range containing an unusual modulation behavior would not only indicate that a significant stream of dark matter is passing through the local neighborhood, but would allow the direction and/or speed of that stream to be determined. However, there may be more than one significant stream or other substructure (in addition to the smooth halo background) so more than one halo component may make significant contributions to the recoil spectrum and modulation signals, complicating the interpretation of modulation data. We turn to a multiple component halo next.

C. Multiple component halo

Thus far we have considered the modulation spectra of individual components of the dark matter halo separately.

However, in greater likelihood, the local dark matter will be comprised of a combination of virialized and unvirialized components. In such cases, low-velocity dark matter will most likely be in equilibrium and well described by a smooth halo, while the high-velocity tail of the distribution may have additional contributions from streams or debris flows. The resulting modulation spectrum will be a linear combination of the spectra shown in Fig. 3, appropriately weighted by the relative density of each component. A general study of dark matter detection in the presence of arbitrary streams or debris flow, in combination with a smooth halo background, can be found in Savage, Freese, and Gondolo (2006) and Kuhlen, Lisanti, and Spergel (2012).

The addition of even a small amount of substructure to the smooth halo background can significantly alter the observational signals in direct detection experiments from those due to the background distribution alone. We take, for example, the case of the SHM with the addition of our example (Sgr-motivated) stream at a density of 10% that of the SHM. While the overall recoil spectrum is approximately exponentially falling due to the large contribution from the SHM, a noticeable dropoff in the spectrum appears around a characteristic energy E_c corresponding to the step in the stream contribution. The impact on the modulation, shown in Fig. 4, is even more pronounced. As can be seen in the middle panel, the shape can differ significantly from that due to either contribution alone: the modulation is no longer sinusoidal and is not even symmetric in time. The phase also differs significantly: the peak of the modulation occurs at a time several months different from that of either component. From the different panels, it is also clear that the phase changes with recoil energy by more than just a 180° phase flip.

In the general case where multiple components contribute significantly to the scattering, the following features in the modulation spectrum can arise:

- The phase of modulation can vary strongly with recoil energy and not just by a 180° phase reversal.
- The combined modulation may not be sinusoidal, even if the modulation of each individual component is.
- The combined modulation may not be time symmetric, even if the modulation of each individual component is.
- The minimum and maximum recoil rates do not necessarily occur 0.5 yr apart.

More quantitatively, the time dependence of the rate is no longer dominated by the A_1 term in the Fourier expansion of Eq. (28), and other terms in the expansion contribute. A power spectrum of the modulation is very useful for understanding the relative strengths of these higher-order contributions [see, e.g., Chang, Pradler, and Yavin (2012)]. The DAMA experiment is currently the only one with enough data to have produced a power spectrum of their results; their measured limit on A_2/A_1 can already provide constraints on certain types of streams as has been shown for the case of inelastic dark matter in Alves, Lisanti, and Wacker (2010).

IV. EXPERIMENTAL STATUS OF ANNUAL MODULATION

In this section we discuss the experimental status of dark matter annual modulation searches. An extremely diverse set of direct detection experiments exists, which take advantage of a variety of target materials and background rejection techniques. The advantage of such diversity is that different targets are more or less sensitive to different types of dark matter and/or features in the velocity profile. For example, searches for spin-dependent interactions require the use of targets with nonzero spin. Also, a lighter target, such as germanium or sodium versus xenon, is better for detecting light mass dark matter.

The current anomalies from DAMA, CoGeNT, and CRESST have engendered a great deal of excitement in the field, with debates as to whether they represent the first direct observation of dark matter. We now review these experiments as well as their counterparts that report the tightest constraints. We caution that the experimental situation is rapidly changing; the reader should consult more recent literature for the current status of the field.

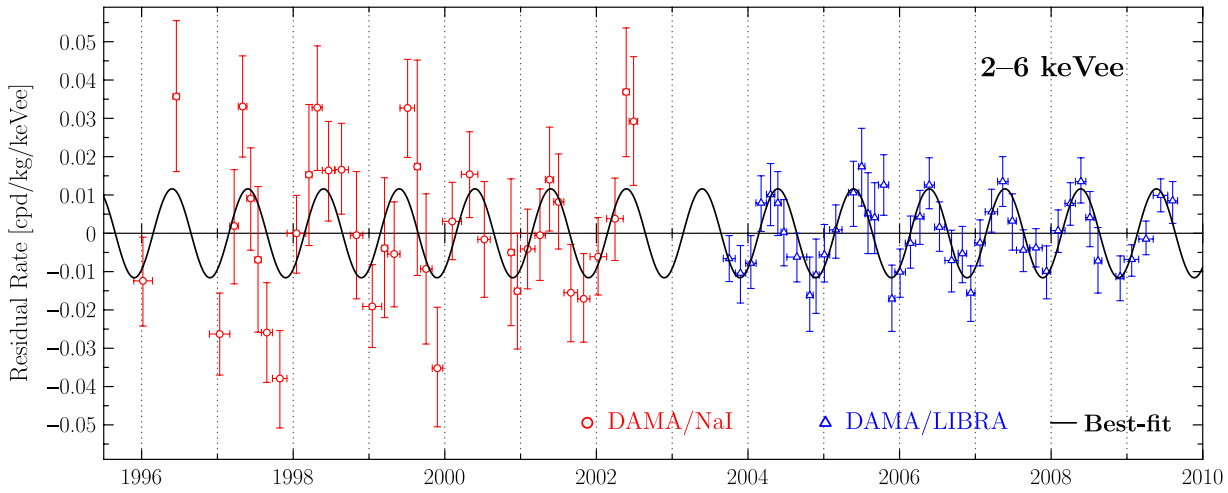

FIG. 5 (color online). The residual rate measured by DAMA/NaI (circles, 0.29 ton yr exposure over 1995–2002) and DAMA/LIBRA (triangles, 0.87 ton yr exposure over 2003–2010) in the 2–6 keVee energy interval, as a function of time. Data are from Bernabei *et al.* (2003, 2010). The solid line is the best-fit sinusoidal modulation $A\cos[(2\pi/T)(t-t_0)]$ with an amplitude $A = 0.0116 \pm 0.0013$ cpd/(kg keV), a phase $t_0 = 0.400 \pm 0.019$ yr (May 26 ± 7 days), and a period $T = 0.999 \pm 0.002$ yr (Bernabei *et al.*, 2010). The data are consistent with the SHM expected phase of 1 June.

A. Experiments and results

1. The DAMA experiment

The Italian Dark Matter Experiment (DAMA) consists of 250 kg of a radio pure NaI(Tl) scintillator. DAMA/NaI (Bernabei *et al.*, 2003) was the first experiment to claim a positive dark matter signal; it was later replaced by DAMA/LIBRA (Bernabei *et al.*, 2008, 2010), which confirmed the results. The experiment has now accumulated 1.17 ton yr of data over 13 years of operation and claims an 8.9σ annual modulation with a phase of May 26 $\pm$ 7 days, consistent with the dark matter expectation (see Fig. 5). The modulation amplitude from 2 to 10 keVee, taken from Bernabei *et al.* (2010), is reproduced in the top panel of Fig. 6. The horizontal axis is given in terms of the electron-equivalent energy E_{ee} in units of keVee, which is related to the nuclear-recoil energy E_{nr} by a multiplicative quenching factor as discussed in Appendix A. The modulation amplitude cannot be given in terms of the nuclear-recoil energy in a model-independent way because the experiment does not distinguish between sodium and iodine recoils on an event-by-event basis and the recoil energy corresponding to a given electron-equivalent energy, related by the nucleus-dependent quenching factor, differs between the two nuclei. In Fig. 6, the presence of a modulation is apparent below ~6 keVee, while the data above ~6 keVee are consistent with zero modulation amplitude.

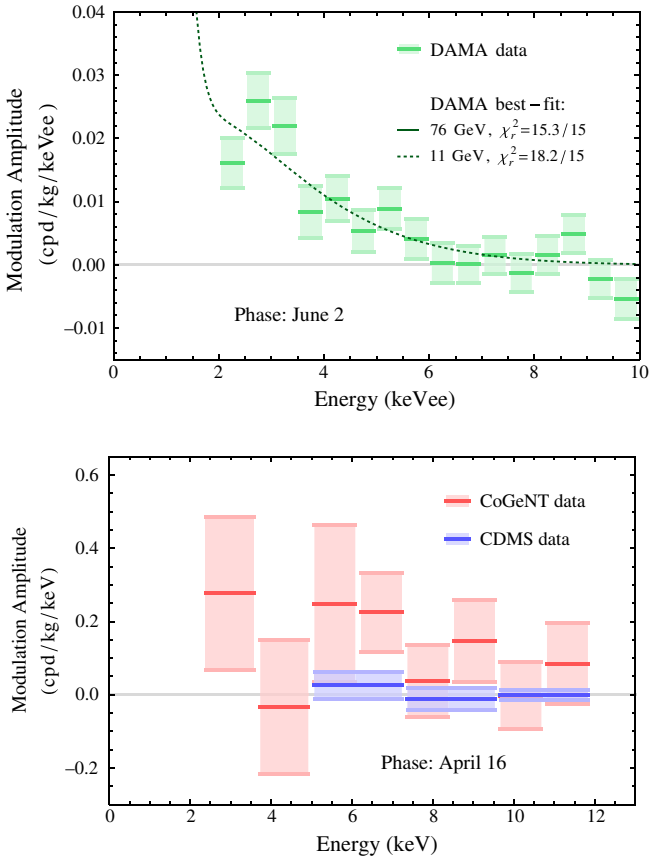

FIG. 6 (color online). The bin-averaged modulation amplitude observed by DAMA (top), CoGeNT (bottom, narrower bins), and CDMS (bottom, wider bins) as a function of energy. Boxes indicate the 1σ uncertainty for each bin. The DAMA results are fit at the SHM expected phase with a peak on 1 June, while the CoGeNT and CDMS bins are given at the CoGeNT best-fit phase with a peak on 16 April. The DAMA data are from Bernabei *et al.* (2010) while the CoGeNT and CDMS binning and results are taken from Ahmed *et al.* (2012). To allow for direct comparison between the two germanium experiments, we present both CoGeNT and CDMS data in keV (nuclear-recoil energy); on the other hand, DAMA data are presented in keVee (electron-equivalent energy). Also shown for DAMA are the best-fit spectra to the data for spin-independent (SI) scattering, corresponding to a WIMP with mass 11 GeV (76 GeV) and SI cross section 2×10^{-4} pb (1.5×10^{-5} pb).

Two possible WIMP masses can reasonably reproduce the observed modulation amplitude spectrum: $m_\chi \sim 10$ GeV (where sodium recoils dominate) and $m_\chi \sim 80$ GeV (where iodine recoils dominate) (Bottino *et al.*, 2003, 2004; Gondolo and Gelmini, 2005; Petriello and Zurek, 2008; Chang, Pierce, and Weiner, 2009; Savage *et al.*, 2009b). The predicted modulation spectra for the two best-fit masses and cross sections, assuming the SHM and SI-only scattering, are shown in Fig. 6. The behavior of the amplitude below the current 2 keVee threshold differs for the two WIMP masses, with the amplitude of the heavy candidate going negative. This is the phase reversal feature in the annual modulation discussed in Sec. III.A. Future iterations of the DAMA experiment, which are expected to have lower thresholds, should be able to distinguish these two possibilities.

The results of the DAMA experiment are in apparent contradiction with the null results from other experiments as discussed below. Other conventional explanations for DAMA's observed annual modulation have also been proposed (Schnee, 2011), including radon contamination and neutrons (Ralston, 2010). The modulating muon flux has been studied as a potential contaminant in the experiment (Blum, 2011; Nygren, 2011; Schnee, 2011; Chang, Pradler, and Yavin, 2012; Fernandez-Martinez and Mahbubani, 2012). Thus far, most of these explanations have been discounted [see Bernabei *et al.* (2012) for a refutation of muons as a significant contaminant], but uncertainty remains.

2. The CoGeNT experiment

The CoGeNT experiment, located in the Soudan mine in Minnesota, consists of 440 g of p-type point-contact (PPC) germanium detectors with a 0.4 keVee energy threshold that makes it particularly well suited to look for light dark matter (Aalseth *et al.*, 2013). Based upon 56 days of exposure, the collaboration reported an excess of low-energy events above the well-known cosmogenic backgrounds (Aalseth *et al.*, 2011a), which could be consistent with a ~10 GeV WIMP (Chang, Liu *et al.*, 2010; Fitzpatrick, Hooper, and Zurek, 2010). After more than a year of data taking, an annual modulation was reported at 2.8σ with a best-fit phase of 16 April (Aalseth *et al.*, 2011b) [see Arina *et al.* (2012) for a Bayesian analysis]. The lower panel of Fig. 6 shows the modulation amplitude observed in the CoGeNT experiment for several energy bins, assuming the best-fit phase; energies have been converted from electron-equivalent to nuclear-recoil energies as described in Appendix A. A significant

modulation is present above 5 keV, which is incompatible with the total rate measured below 4 keV for standard assumptions about the halo and scattering properties (Fox *et al.*, 2012). However, the modulation could be explained by local substructure (Natarajan, Savage, and Freese, 2011; Fox *et al.*, 2012; Kelso, Hooper, and Buckley, 2012).

3. The CDMS experiment

The CDMS experiment also consists of germanium and is located in the Soudan mine. Using the ratio of two signals observed in an interaction with the detector target (phonons and ionization) CDMS can distinguish between nuclear-recoil events (WIMP and/or neutron interactions) and electron-recoil events (beta and gamma interactions), where the latter represents an otherwise dominant background contribution (Akerib *et al.*, 2005). The conventional low-background analyses in CDMS, the most recent having 612 kg days of exposure (Ahmed *et al.*, 2010), have failed to detect any excess events inconsistent with background.

To improve sensitivity to light WIMPs, which produce only low-energy recoils, CDMS has also performed a low-energy analysis (Ahmed *et al.*, 2011), reducing its threshold from 10 to 2 keV. At these lower energies, it is more difficult to discriminate between potential signal events and background events, so there is far more background contamination in this analysis than the conventional case. The ~500 low-energy events found in this analysis are consistent with rough background estimates. However, CDMS places conservative no-background-subtraction constraints on light WIMPs, neglecting background contributions and allowing any or all of the events to be due to WIMPs. CDMS has also performed a modulation search in their low-energy data (Ahmed *et al.*, 2012), finding no evidence for modulation. Constraints on the modulation amplitude, assuming the CoGeNT best-fit phase of 16 April, are shown in the lower panel of Fig. 6. Direct comparison can be made with the CoGeNT modulation results because both experiments have a germanium target, although the CDMS modulation analysis was performed only down to 5 keV, whereas the CoGeNT modulation data go to a much lower ~2 keV.

4. The CRESST experiment

The CRESST experiment, developed at the Max Planck Institute in Munich and deployed in the Gran Sasso Tunnel, has 730 kg days of data with a $CaWO_4$ scintillating crystal target and measures both light and heat to reject electron recoils. It reports an excess of low-energy events with a statistical significance of over 4σ (Angloher *et al.*, 2012). The experiment is not background free however and has experienced problems with energetic alpha and lead ions produced in the decay of polonium, itself produced from radon decay. For various technical reasons not discussed here, polonium deposited in the clamps holding the detectors in place is the major source of such backgrounds. The expected number of these events, which occur on the surface, is determined by extrapolating from high-energy observations (where such background events are readily identifiable) to the signal regions at lower energies using Monte Carlo simulations. Questions have been raised as to whether the Monte Carlo simulations underestimate the background contamination by failing to account for the roughness of the surface at microscopic scales (Kuzniak, Boulay, and Pollmann, 2012). An upcoming redesign should eliminate this background source, and future CRESST runs should clarify the origin of the current excess.

5. The XENON experiment

The XENON Collaboration has developed a series of liquid xenon target experiments, with the most recent iteration (XENON100) containing ~100 kg of xenon (Aprile *et al.*, 2012c). As with CDMS and CRESST, XENON uses two signals (scintillation and ionization in this case) to discriminate between nuclear recoils and electron recoils. XENON100 and XENON10 both performed conventional low-background analyses (Angle *et al.*, 2008; Aprile *et al.*, 2012b). In addition, XENON10 published a low-energy analysis that sacrifices background discrimination to improve sensitivity to light WIMP masses (Angle *et al.*, 2011). None of these analyses find an excess of events above expected background and XENON100 currently places the most stringent constraints on the SI cross section for WIMPs heavier than ~10 GeV.

6. Other experiments

The experiments discussed in detail here represent only a fraction of the current direct detection program. No other experiment claims an excess of events consistent with dark matter and, for standard assumptions, none provide constraints as stringent as those from CDMS and XENON100. One exception is the case of SD scattering where the coupling to the neutron is suppressed relative to the proton ($a_n \ll a_p$). The proton-even target materials in CDMS and XENON couple only weakly to the WIMP in this case [see Eq. (11)], so these experiments place relatively weak constraints. For this case, COUPP (Behnke *et al.*, 2012), PICASSO (Archambault *et al.*, 2012), and SIMPLE (Felizardo *et al.*, 2012) provide the best limits.

B. Compatibility of experimental results

Figure 7 summarizes the current status of anomalies and limits for SI scattering, assuming the SHM with $v_0 = 220$ km/s and $v_{esc} = 550$ km/s. Note that the experimental limits and anomalies, as shown in this figure, are highly dependent on the assumptions made about the particle and astrophysics [see Fox, Kribs, and Tait, 2011; Fox, Liu, and Weiner, 2011; Herrero-Garcia, Schwetz, and Zupan, 2012a; Herrero-Garcia, Schwetz, and Zupan, 2012b for astrophysics-independent comparisons]. The compatibility may change for, e.g., a different WIMP-nucleus effective operator or for additional substructure contributions (Fairbairn and Schwetz, 2009; Farina *et al.*, 2011; Fornengo, Panci, and Regis, 2011; Frandsen *et al.*, 2011; Schwetz and Zupan, 2011; Arina *et al.*, 2012). However, note that changes to the particle physics and/or astrophysics may change the interpretation of individual results without actually affecting the

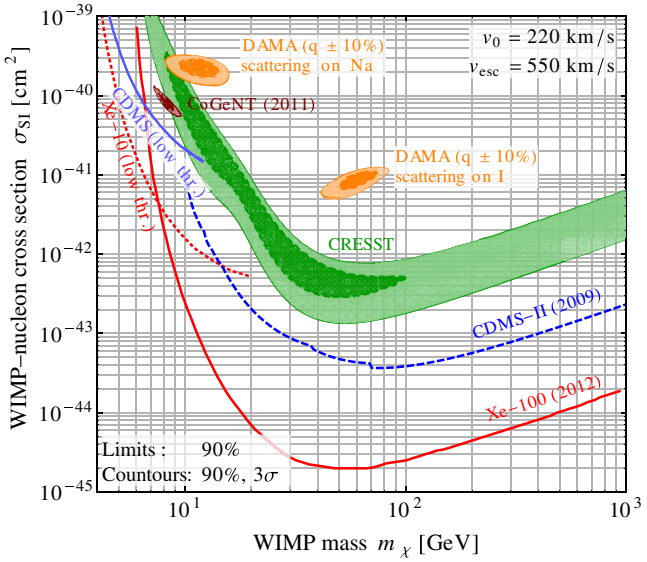

FIG. 7 (color online). WIMP mass and SI cross sections consistent with the anomalies seen by DAMA, CoGeNT, and CRESST, as well as constraints placed by the null results of CDMS and XENON (as of summer 2012). The halo model is assumed to be the SHM with the given parameters. The lack of overlap between the regions of the three anomalous results and their locations above the exclusion curves of CDMS and XENON indicate a conflict between the experimental results in this case. Alternative couplings, modified halo models, and systematic issues have been proposed to reconcile this apparent incompatibility. Figure courtesy of J. Kopp (Kopp, Schwetz, and Zupan, 2012).

compatibility among different results.[11] In addition, various systematic issues regarding the behavior of individual detectors, such as the calibration of the recoil-energy scale, can impact the interpretation of experimental results.[12]

The high-mass $\mathcal{O}$(80 GeV) DAMA region appears to be ruled out for both SI and SD elastic scattering by null results from CDMS, XENON, and COUPP—a heavy mass WIMP is viable only for nonstandard interactions. On the other hand, the compatibility of light $\mathcal{O}$(10 GeV) dark matter remains the subject of some debate. For the case of SI scattering, these positive results are in apparent contradiction with each other and with CDMS and XENON. Some have nevertheless argued that some of the results could potentially be reconciled [see, e.g., Hooper *et al.* (2010) and Collar and Fields (2012)].

For the case of SD scattering, the DAMA lower mass region has until recently remained compatible with all experiments (Ullio, Kamionkowski, and Vogel, 2001; Savage, Gondolo, and Freese, 2004; Savage *et al.*, 2009b), provided the SD coupling to the neutron is strongly suppressed relative to the proton ($|a_n| \ll |a_p|$). Results from PICASSO have since closed this window for standard assumptions (Archambault *et al.*, 2012). This particular case is also uniquely suited to be probed by indirect searches involving detection of neutrinos produced by WIMPs annihilating in the Sun, e.g., with the Super-Kamiokande (Desai *et al.*, 2004) and IceCube detectors (Abbasi *et al.*, 2012).

C. Future prospects

Direct detection experiments are poised at an important juncture. In the past few years, the cross sections reached by the detectors have improved by roughly 2 orders of magnitude. A similar improvement is expected in the next generation of detectors, which will be 1 ton (1000 kg) in size. These experiments probe some of the most promising regions of WIMP parameter space, exploring Higgs exchange cross sections and large regions of supersymmetric parameter space. However, as the sensitivity of direct detection experiments reaches $\sigma_{p,\mathrm{SI}} \sim 10^{-47}$ cm^2, astrophysical neutrinos become an irreducible background, so the experiments are no longer zero background (Monroe and Fisher, 2007; Strigari, 2009; Gutlein *et al.*, 2010). In addition to ton-size detectors pushing the reach to lower cross sections and heavier dark matter masses, efforts are also being made to explore dark matter with masses below ~1 GeV using electron recoils (Essig *et al.*, 2012; Essig, Mardon, and Volansky, 2012).

New technology and creative experimental designs allow for further exploration of the $\mathcal{O}$(10 GeV) dark matter anomalies. For example, KIMS (Kim *et al.*, 2012) and ANAIS (Amare *et al.*, 2011), which use CsI(Tl) and NaI(Tl) targets, respectively, will test the DAMA modulation claim. DM-Ice (Cherwinka *et al.*, 2012) is a detector located at the South Pole that also uses the same target material as DAMA. Because it is located in the southern hemisphere and is embedded deep in the ice where the natural temperature variation is minimal, DM-Ice should have different environmental background sources than DAMA.

In addition, directional detectors provide a powerful probe in mapping out the distribution of the local dark matter. Whereas the modulation in the recoil rate discussed throughout this Colloquium resulted from the variation in the velocity of the detector relative to the dark matter halo (due to the Earth orbiting the Sun and, to a much lesser extent, the rotation of the Earth), detectors with recoil direction sensitivity observe a diurnal modulation in the recoil direction due to the rotation of the detector as the Earth spins (i.e., the orientation of the detector with respect to the halo changes throughout the day). The incoming WIMP flux is peaked in the direction of the Sun's motion and, as a result, the nuclear-recoil angular spectrum is peaked in the opposite direction for most energies. Therefore, the event rate experiences a strong forward-backward ("head-tail") asymmetry along the direction of the disk rotation. In addition, the direction of the dark matter wind as observed in the laboratory frame changes with the time of day due to the Earth's daily rotation. The result is a differential recoil rate at a particular angle (as measured in the laboratory frame) that diurnally modulates with an

[11]Newer measurements of the Sun's velocity relative to the galactic halo [as high as 250 km/s (Reid *et al.*, 2009), as opposed to the canonical 220 km/s in common use] shifts the best-fit regions and the limit curves to the left. For the SHM, the regions compatible with DAMA, CoGeNT, and CRESST move down in mass by a few GeV (Savage *et al.*, 2009a). Because the bounds from the null experiments move to lower masses as well, the discrepancy between experiments is not alleviated.

[12]Considerable discussion remains as to the true sensitivity of the XENON experiment near the energy threshold [see, e.g., Collar and McKinsey (2010) and Savage *et al.* (2011)].

amplitude as large as ~100% (Spergel, 1988; Gondolo, 2002), far larger than the modulation effects that are the focus of this Colloquium. Ahlen *et al.* (2010) reviewed the current status of prototypes of directional detection experiments. To achieve reasonable angular resolution, the recoiling nucleus must leave a track that is sufficiently long. As a result, the chosen detector material is a gas, typically CF_4 and CS_2 in current designs. The use of gas as the active target, with the gas being at low pressure (well below atmospheric pressure to allow for longer recoil tracks), will require these detectors to have volumes of $\mathcal{O}(10^4\ \mathrm{m}^3)$ to achieve ton-scale masses.

A novel type of directional detector has also recently been proposed that uses a DNA tracking material (Drukier *et al.*, 2012). These detectors can achieve nanometer resolution with an energy threshold of 0.5 keV and can operate at room temperature. When a WIMP from the galactic halo elastically scatters off of a nucleus in the detector, the recoiling nucleus then traverses thousands of strings of single stranded DNA (ssDNA) and severs those ssDNA strings it hits. The location of the break can be identified by amplifying and identifying the segments of cut ssDNA using techniques well known to biologists. Thus, the path of the recoiling nucleus can be tracked to nanometer accuracy. By leveraging advances in molecular biology, the goal is to achieve about 1000-fold better spatial resolution than in conventional WIMP detectors at a reasonable cost.

Directional detectors are particularly useful in mapping out the local dark matter distribution (Copi, Heo, and Krauss, 1999; Copi and Krauss, 2001; Morgan, Green, and Spooner, 2005; Alenazi and Gondolo, 2008; Alves, Hedri, and Wacker, 2012; Bozorgnia, Gelmini, and Gondolo, 2012; Lee and Peter, 2012). A positive signal at both a direct and a directional detection experiment would provide complementary information about the halo, building our understanding of the velocity structure of the local dark matter.

V. SUMMARY

The theoretical and experimental status of the annual modulation of a dark matter signal (due to the Earth's rotation around the Sun) in direct detection experiments has been reviewed. Annual modulation provides an important method of discriminating a signal from most backgrounds, which do not experience such a yearly variation. The Milky Way halo consists of a dominant smooth component as well as substructures such as streams, tidal debris, and/or a dark disk, each of which contributes to the modulation of the signal. In the standard halo model, the count rate in experiments should peak in June with a minimum in December; substructure may change the phase, shape, and amplitude of the modulation. The current experimental situation is puzzling, as several experiments have positive signals (DAMA and CoGeNT both see annual modulation, while CoGeNT and CRESST-II have unexplained events) but appear to be contradicted by null results from other experiments (CDMS and XENON). In the future, detectors with sensitivity to the directionality of WIMPs should enable determination of the direction of the WIMP wind as well as diurnal modulation due to the Earth's rotation. Proposed techniques for directional detection include large gaseous detectors as well as nanometer tracking with DNA. Consistent measurement of a head-tail asymmetry together with annual modulation would provide convincing evidence of WIMP detection. The future of dark matter searches is promising and an annual modulation signal should play an important role in the interpretation and confirmation of a potential WIMP signal.

ACKNOWLEDGMENTS

K. F. thanks M. Valluri and M. Zemp for useful conversations. K. F. acknowledges the support of the DOE and the Michigan Center for Theoretical Physics via the University of Michigan. K. F. thanks the Caltech Physics Department for hospitality and support during her sabbatical. K. F. is supported as a Simons Foundation Fellow in Theoretical Physics. M. L. is supported by the Simons Postdoctoral Fellows Program and the U.S. National Science Foundation, Grant No. NSF-PHY-0705682, and the LHC Theory Initiative. C. S. is grateful for financial support from the Swedish Research Council (VR) through the Oskar Klein Centre. C. S. thanks the Department of Physics & Astronomy at the University of Utah for support. K. F. and M. L. acknowledge the hospitality of the Aspen Center for Physics, which is supported by the National Science Foundation Grant No. PHY-1066293.

APPENDIX A: QUENCHING FACTOR

Any experimental apparatus does not directly measure the recoil energy of scattering events. The recoiling nucleus (or recoiling electron, in the case of some backgrounds) will transfer its energy to either electrons, which may be observed as, e.g., ionization or scintillation in the detector, or to other nuclei, producing phonons and heat; these are the signatures that are measured. Some experiments that measure only scintillation or ionization give their results in terms of the electron-equivalent energy E_{ee} of an event in their detector (usually given in units of keVee). This quantity is defined as the energy of an electron recoil that would produce the observed amount of scintillation or ionization, even if the event was actually a nuclear recoil rather than an electron recoil. Nuclear recoils tend to produce a smaller amount of scintillation or ionization than electron recoils for the same recoil energy, so E_{ee} is not the recoil energy of that event if it is a nuclear-recoil event. For nuclear recoils, these two energies are related by $E_{\mathrm{ee}} = QE_{\mathrm{nr}}$, where Q is called the quenching factor. The quenching factor is different for each element in a detector and can have a recoil-energy dependence. The different quenching factors for different elements and for electron-recoil events ($Q = 1$ for electron recoils, by definition) makes it impossible to determine the recoil energy of an event based upon the scintillation or ionization signal alone.

Take, for example, the NaI in DAMA, with $Q_{\mathrm{Na}} \approx 0.3$ and $Q_{\mathrm{I}} \approx 0.09$ (Bernabei *et al.*, 1996) [see Tretyak (2010) and references therein for quenching factor measurements of NaI and several other scintillators used in direct detection experiments]. A recoil event in DAMA that produces 2 keVee of scintillation can be from a ~7 keV Na recoil, a ~22 keV I recoil, or a 2 keV electron recoil. DAMA is unable to distinguish between these three types of events on an

event-by-event basis, so any DAMA analysis is necessarily based upon the total dR/dE_{ee} spectrum that contains contributions from all three types of events.

CoGeNT, which observes only ionization in a germanium target, also gives results in terms of the electron-equivalent energy spectrum. CoGeNT suggests using $Q(E_{nr}) = 0.199\,35 E_{nr}^{0.1204}$ as a reasonable approximation to the quenching factor measurements over the energy range of interest (Collar, 2012) [measurements of Q in germanium can be found in the Appendix of Lin *et al.* (2009)]. CDMS, which also uses a germanium target, can discriminate between electron-recoil and nuclear-recoil events and can reconstruct the nuclear recoil (although limited by a finite resolution), so results for this experiment are given in terms of $E \approx E_{nr}$ rather than E_{ee}. Because CDMS and CoGeNT are made of the same target material, one would expect that these two experiments should have the same nuclear-recoil spectrum; however, one should keep in mind the caveat that the two results are given in terms of different quantities that must be rescaled to make direct comparisons between their two results.

APPENDIX B: MEAN INVERSE SPEEDS OF COMMONLY USED VELOCITY DISTRIBUTIONS

The detection rate in dark matter experiments is directly proportional to the mean inverse speed

$$\eta(v_{min}) = \int_{|\mathbf{v}|>v_{min}} d^3v \frac{f(\mathbf{v}, t)}{v}.$$

Here we present analytical results of this integration quantity for several commonly used isotropic velocity distributions. We define $\tilde{f}(\mathbf{v})$ as the velocity distribution in the rest frame of the dark matter population [i.e., $\int d^3v \mathbf{v} \tilde{f}(\mathbf{v}) = \mathbf{0}$]. The velocity distribution in the laboratory frame is determined via the Galilean transformation $f(\mathbf{v}) = \tilde{f}(\mathbf{v}_{obs} + \mathbf{v})$, where $\mathbf{v}_{obs}(t)$ is the (time-dependent) motion of the laboratory (observer) relative to the rest frame of the dark matter population. This motion is described in more detail in Sec. III.

The distributions considered below are Maxwellian distributions (including two modifications to account for a finite cutoff) and distributions corresponding to cold flows and debris flows. These are not the only possible distributions of dark matter and may be only simple approximations for some populations, but they are frequently used distributions that have known analytical forms for η.

1. Maxwellian distributions

Perhaps the most useful simple distribution is the Maxwellian:

$$\tilde{f}(\mathbf{v}) = \left(\frac{1}{\pi v_0^2}\right)^{3/2} e^{-\mathbf{v}^2/v_0^2}. \tag{B1}$$

For this distribution,

$$\eta(v_{min}, t) = \frac{1}{2v_{obs}}[\mathrm{erf}(x + y) - \mathrm{erf}(x - y)], \tag{B2}$$

where v_0 is the most probable speed,

$$x \equiv v_{min}/v_0 \quad \text{and} \quad y \equiv v_{obs}/v_0. \tag{B3}$$

Many well-mixed populations of dark matter particles can be expected to have a Maxwellian or Maxwellian-like distribution, in which case the above is a useful first approximation.

The SHM takes the dark matter halo to be an isothermal sphere, in which case the velocity distribution is Maxwellian. However, high-velocity particles would escape the Galaxy, so the high-velocity tail of the distribution is cut off in a realistic halo model. Section II.B.1 presents two methods for removing the tail of the Maxwellian, with the resulting distributions given by Eqs. (14) and (17). For the SHM or any dark matter component described by one of these two velocity distributions, the mean inverse speed η is (Savage, Freese, and Gondolo, 2006; McCabe, 2010)

$$\eta(v_{min}) = \begin{cases} \frac{1}{v_{obs}}, & \text{for } z < y, x < |y - z|, \\ \frac{1}{2N_{esc} v_{obs}}[\mathrm{erf}(x+y) - \mathrm{erf}(x-y) - \frac{4}{\sqrt{\pi}}(1 - \beta(x^2 + \frac{1}{3}y^2 - z^2))ye^{-z^2}], & \text{for } z > y, x < |y - z|, \\ \frac{1}{2N_{esc} v_{obs}}[\mathrm{erf}(z) - \mathrm{erf}(x-y) - \frac{2}{\sqrt{\pi}}(y + z - x - \frac{1}{3}\beta(y - 2z - x)(y + z - x)^2)e^{-z^2}], & \text{for } |y - z| < x < y + z, \\ 0, & \text{for } y + z < x, \end{cases} \tag{B4}$$

where $\beta = 0$ for Eq. (14) and $\beta = 1$ for Eq. (17), x and y are as defined above, and

$$z \equiv v_{esc}/v_0. \tag{B5}$$

Note that the normalization factor N_{esc} has a different form for the two distributions.

2. Cold flow

Cold flows, such as tidal streams, have small to negligible velocity dispersions. In the case of zero dispersion,

$$\tilde{f}(\mathbf{v}) = \delta^3(\mathbf{v}) \tag{B6}$$

and

$$\eta(v_{min}) = \frac{1}{v_{obs}} \theta(v_{obs} - v_{min}), \tag{B7}$$

where θ is the Heaviside function. Although the velocity dispersion is small in cold flows, in some cases such as tidal streams it is not completely negligible. In those cases, a useful approximation can often be made with the Maxwellian distribution of Eq. (B1) with a small v_0.

3. Debris flow

To first order, the debris flow in a Milky Way-like galaxy (Lisanti and Spergel, 2012) has an isotropic, constant-speed velocity distribution in the galactic rest frame that can be described by a delta function in *speed*, as opposed to the delta function in *velocity* seen with cold flows above:

$$\tilde{f}(\mathbf{v}) = \frac{1}{4\pi v_{\rm flow}^2}\delta(|\mathbf{v}| - v_{\rm flow}), \tag{B8}$$

where $v_{\rm flow}$ is the uniform speed of the particles. In the laboratory frame (Kuhlen, Lisanti, and Spergel, 2012),

$$\eta(v_{\rm min}) = \begin{cases} \frac{1}{v_{\rm flow}}, & \text{for } v_{\rm min} < v_{\rm flow} - v_{\rm obs}, \\ \frac{1}{2v_{\rm flow}v_{\rm obs}}[v_{\rm flow} + v_{\rm obs} - v_{\rm min}], & \text{for } v_{\rm flow} - v_{\rm obs} < v_{\rm min} < v_{\rm flow} + v_{\rm obs}, \\ 0, & \text{for } v_{\rm flow} + v_{\rm obs} < v_{\rm min}. \end{cases} \tag{B9}$$

Although the debris flow has both a dispersion in the speed and some anisotropy in the galactic rest frame, the above reference shows that this analytical form still provides a reasonable approximation.

REFERENCES

Aalseth, C., *et al.* (CoGeNT Collaboration), 2011a, Phys. Rev. Lett. **106**, 131301.
Aalseth, C., *et al.* (CoGeNT Collaboration), 2011b, Phys. Rev. Lett. **107**, 141301.
Aalseth, C., *et al.* (CoGeNT Collaboration), 2013, Phys. Rev. D **88**, 012002.
Abbasi, R., *et al.* (IceCube Collaboration), 2012, Phys. Rev. D **85**, 042002.
Acciarri, R., *et al.*, 2011, J. Phys. Conf. Ser. **308**, 012005.
Ahlen, S., *et al.*, 1987, Phys. Lett. B **195**, 603.
Ahlen, S., *et al.*, 2010, Int. J. Mod. Phys. A **25**, 1.
Ahmed, Z., *et al.* (CDMS-II Collaboration), 2010, Science **327**, 1619.
Ahmed, Z., *et al.* (CDMS-II Collaboration), 2011, Phys. Rev. Lett. **106**, 131302.
Ahmed, Z., *et al.* (CDMS Collaboration), 2012, arXiv:1203.1309.
Akerib, D., *et al.* (CDMS Collaboration), 2005, Phys. Rev. D **72**, 052009.
Akimov, D. Y., *et al.*, 2007, Astropart. Phys. **27**, 46.
Akimov, D. Y., *et al.*, 2012, Phys. Lett. B **709**, 14.
Alenazi, M. S., and P. Gondolo, 2008, Phys. Rev. D **77**, 043532.
Alner, G., *et al.*, 2005, Nucl. Instrum. Methods Phys. Res., Sect. A **555**, 173.
Alner, G., *et al.* (UK Dark Matter Collaboration), 2005, Phys. Lett. B **616**, 17.
Alves, D. S., S. R. Behbahani, P. Schuster, and J. G. Wacker, 2010, Phys. Lett. B **692**, 323.
Alves, D. S., S. E. Hedri, and J. G. Wacker, 2012, arXiv:1204.5487.
Alves, D. S., M. Lisanti, and J. G. Wacker, 2010, Phys. Rev. D **82**, 031901.
Amare, J., *et al.*, 2011, Proc. Sci. IDM2010, 020.
An, H., S.-L. Chen, R. N. Mohapatra, S. Nussinov, and Y. Zhang, 2010, Phys. Rev. D **82**, 023533.
Angle, J., *et al.* (XENON Collaboration), 2008, Phys. Rev. Lett. **100**, 021303.
Angle, J., *et al.* (XENON10 Collaboration), 2011, Phys. Rev. Lett. **107**, 051301.
Angloher, G., *et al.*, 2012, Eur. Phys. J. C **72**, 1971.
Aprile, E., *et al.* (XENON100 Collaboration), 2011a, Phys. Rev. D **84**, 061101.
Aprile, E., *et al.* (XENON Collaboration), 2011b, Astropart. Phys. **34**, 679.
Aprile, E., *et al.* (XENON1T Collaboration), 2012a, arXiv:1206.6288.
Aprile, E., *et al.* (XENON100 Collaboration), 2012b, Phys. Rev. Lett. **109**, 181301.
Aprile, E., *et al.* (XENON100 Collaboration), 2012c, Astropart. Phys. **35**, 573.
Archambault, S., *et al.* (PICASSO Collaboration), 2012, Phys. Lett. B **711**, 153.
Arina, C., J. Hamann, R. Trotta, and Y. Y. Wong, 2012, J. Cosmol. Astropart. Phys. 03, 008.
Armengaud, E., *et al.* (EDELWEISS Collaboration), 2011, Phys. Lett. B **702**, 329.
Armengaud, E., *et al.* (EDELWEISS Collaboration), 2012, Phys. Rev. D **86**, 051701.
Babcock, H. W., 1939, Lick Obs. Bull. **19**, 41.
Barnabe-Heider, M., *et al.* (PICASSO Collaboration), 2005, Nucl. Instrum. Methods Phys. Res., Sect. A **555**, 184.
Baushev, A., 2013, Astrophys. J. **771**, 117.
Bednyakov, V., and F. Simkovic, 2005, Phys. Part. Nucl. **36**, 131.
Bednyakov, V., and F. Simkovic, 2006, Phys. Part. Nucl. **37**, S106.
Behnke, E., *et al.* (COUPP Collaboration), 2012, Phys. Rev. D **86**, 052001.
Belokurov, V., *et al.*, 2006, Astrophys. J. **642**, L137.
Bergstrom, L., 2000, Rep. Prog. Phys. **63**, 793.
Bernabei, R., *et al.*, 2012, Eur. Phys. J. C **72**, 2064.
Bernabei, R., *et al.*, 1996, Phys. Lett. B **389**, 757.
Bernabei, R., *et al.*, 2003, Riv. Nuovo Cimento **26N1**, 1.
Bernabei, R., *et al.* (DAMA Collaboration), 2008, Nucl. Instrum. Methods Phys. Res., Sect. A **592**, 297.
Bernabei, R., *et al.* (DAMA Collaboration, LIBRA Collaboration), 2010, Eur. Phys. J. C **67**, 39.
Bertone, G., D. Hooper, and J. Silk, 2005, Phys. Rep. **405**, 279.
Bertschinger, E., 1985, Astrophys. J. Suppl. Ser. **58**, 1.
Blum, K., 2011, arXiv:1110.0857.
Bottino, A., F. Donato, N. Fornengo, and S. Scopel, 2003, Phys. Rev. D **68**, 043506.
Bottino, A., F. Donato, N. Fornengo, and S. Scopel, 2004, Phys. Rev. D **69**, 037302.
Bovy, J., D. W. Hogg, and H.-W. Rix, 2009, Astrophys. J. **704**, 1704.
Bovy, J., and S. Tremaine, 2012, Astrophys. J. **756**, 89.
Bozorgnia, N., G. B. Gelmini, and P. Gondolo, 2012, J. Cosmol. Astropart. Phys. 06, 037.
Bruch, T., J. Read, L. Baudis, and G. Lake, 2009, Astrophys. J. **696**, 920.
Caldwell, J., and J. Ostriker, 1981, Astrophys. J. **251**, 61.

Carlin, J. L., *et al.*, 2012, Astrophys. J. **744**, 25.
Catena, R., and P. Ullio, 2010, J. Cosmol. Astropart. Phys. 08, 004.
Chang, S., J. Liu, A. Pierce, N. Weiner, and I. Yavin, 2010, J. Cosmol. Astropart. Phys. 08, 018.
Chang, S., A. Pierce, and N. Weiner, 2009, Phys. Rev. D **79**, 115011.
Chang, S., A. Pierce, and N. Weiner, 2010, J. Cosmol. Astropart. Phys. 01, 006.
Chang, S., J. Pradler, and I. Yavin, 2012, Phys. Rev. D **85**, 063505.
Chang, S., N. Weiner, and I. Yavin, 2010, Phys. Rev. D **82**, 125011.
Chaudhury, S., P. Bhattacharjee, and R. Cowsik, 2010, J. Cosmol. Astropart. Phys. 09, 020.
Cherwinka, J., *et al.*, 2012, Astropart. Phys. **35**, 749.
Cirigliano, V., M. L. Graesser, and G. Ovanesyan, 2012, J. High Energy Phys. 10, 025.
Collar, J., 2012 (private communication).
Collar, J., and N. Fields, 2012, arXiv:1204.3559.
Collar, J., and D. McKinsey, 2010, arXiv:1005.0838.
Copi, C. J., J. Heo, and L. M. Krauss, 1999, Phys. Lett. B **461**, 43.
Copi, C. J., and L. M. Krauss, 2001, Phys. Rev. D **63**, 043507.
Coron, N., *et al.*, 2011, Proc. Sci., IDM2010, 054.
Daw, E., *et al.*, 2012, Astropart. Phys. **35**, 397.
Debattista, V. P., *et al.*, 2008, Astrophys. J. **681**, 1076.
Desai, S., *et al.* (Super-Kamiokande Collaboration), 2004, Phys. Rev. D **70**, 083523.
Diemand, J., M. Kuhlen, and P. Madau, 2007, Astrophys. J. **657**, 262.
Diemand, J., *et al.*, 2008, Nature (London) **454**, 735.
Dohm-Palmer, R., *et al.*, 2001, Astrophys. J. **555**, L37.
Drees, M., and C.-L. Shan, 2007, J. Cosmol. Astropart. Phys. 06, 011.
Drees, M., and C.-L. Shan, 2008, J. Cosmol. Astropart. Phys. 06, 012.
Drukier, A., K. Freese, and D. Spergel, 1986, Phys. Rev. D **33**, 3495.
Drukier, A., and L. Stodolsky, 1984, Phys. Rev. D **30**, 2295.
Drukier, A., *et al.*, 2012, arXiv:1206.6809.
Dubinski, J., and R. Carlberg, 1991, Astrophys. J. **378**, 496.
Duda, G., A. Kemper, and P. Gondolo, 2007, J. Cosmol. Astropart. Phys. 04, 012.
Duffy, L., and P. Sikivie, 2008, Phys. Rev. D **78**, 063508.
Essig, R., A. Manalaysay, J. Mardon, P. Sorensen, and T. Volansky, 2012, Phys. Rev. Lett. **109**, 021301.
Essig, R., J. Mardon, and T. Volansky, 2012, Phys. Rev. D **85**, 076007.
Faber, S., and J. Gallagher, 1979, Annu. Rev. Astron. Astrophys. **17**, 135.
Fairbairn, M., and T. Schwetz, 2009, J. Cosmol. Astropart. Phys. 01, 037.
Fan, J., M. Reece, and L.-T. Wang, 2010, J. Cosmol. Astropart. Phys. 11, 042.
Farina, M., D. Pappadopulo, A. Strumia, and T. Volansky, 2011, J. Cosmol. Astropart. Phys. 11, 010.
Feldstein, B., A. L. Fitzpatrick, and E. Katz, 2010, J. Cosmol. Astropart. Phys. 01, 020.
Felizardo, M., *et al.* (SIMPLE Collaboration), 2012, Phys. Rev. Lett. **108**, 201302.
Feng, J. L., J. Kumar, D. Marfatia, and D. Sanford, 2011, Phys. Lett. B **703**, 124.
Fernandez-Martinez, E., and R. Mahbubani, 2012, J. Cosmol. Astropart. Phys. 07, 029.
Fillmore, J., and P. Goldreich, 1984, Astrophys. J. **281**, 1.
Fiorentin, P. R., M. G. Lattanzi, R. L. Smart, A. Spagna, C. A. L. Bailer-Jones, T. C. Beers, and T. Zwitter, 2010, EAS Publ. Ser. **45**, 203.
Fitzpatrick, A. L., W. Haxton, E. Katz, N. Lubbers, and Y. Xu, 2013, J. Cosmol. Astropart. Phys. 02, 004.
Fitzpatrick, A. L., D. Hooper, and K. M. Zurek, 2010, Phys. Rev. D **81**, 115005.
Fornengo, N., P. Panci, and M. Regis, 2011, Phys. Rev. D **84**, 115002.
Fox, P. J., J. Kopp, M. Lisanti, and N. Weiner, 2012, Phys. Rev. D **85**, 036008.
Fox, P. J., G. D. Kribs, and T. M. Tait, 2011, Phys. Rev. D **83**, 034007.
Fox, P. J., J. Liu, and N. Weiner, 2011, Phys. Rev. D **83**, 103514.
Frandsen, M. T., *et al.*, 2011, Phys. Rev. D **84**, 041301.
Freese, K., J. A. Frieman, and A. Gould, 1988, Phys. Rev. D **37**, 3388.
Freese, K., P. Gondolo, and H. J. Newberg, 2005, Phys. Rev. D **71**, 043516.
Freese, K., P. Gondolo, H. J. Newberg, and M. Lewis, 2004, Phys. Rev. Lett. **92**, 111301.
Freese, K., P. Gondolo, and L. Stodolsky, 2001, Phys. Rev. D **64**, 123502.
Freese, K., and C. Savage, 2012, Phys. Lett. B **717**, 25.
Gelmini, G., and P. Gondolo, 2001, Phys. Rev. D **64**, 023504.
Gondolo, P., 2002, Phys. Rev. D **66**, 103513.
Gondolo, P., and G. Gelmini, 2005, Phys. Rev. D **71**, 123520.
Gong, H., K. Giboni, X. Ji, A. Tan, and L. Zhao, 2013, JINST **8**, P01002.
Goodman, M. W., and E. Witten, 1985, Phys. Rev. D **31**, 3059.
Green, A. M., 2001, Phys. Rev. D **63**, 043005.
Green, A. M., 2002, Phys. Rev. D **66**, 083003.
Green, A. M., 2003, Phys. Rev. D **68**, 023004.
Green, A. M., 2010, J. Cosmol. Astropart. Phys. 10, 034.
Green, A. M., 2012, Mod. Phys. Lett. A **27**, 1230004.
Gunn, J. E., and I. Gott, J. Richard, 1972, Astrophys. J. **176**, 1.
Gutlein, A., *et al.*, 2010, Astropart. Phys. **34**, 90.
Hall, C., *et al.*, 2010, Proc. Sci., ICHEP2010, 431.
Hansen, S. H., D. Egli, L. Hollenstein, and C. Salzmann, 2005, New Astron. **10**, 379.
Hansen, S. H., B. Moore, M. Zemp, and J. Stadel, 2006, J. Cosmol. Astropart. Phys. 01, 014.
Helm, R. H., 1956, Phys. Rev. **104**, 1466.
Herrero-Garcia, J., T. Schwetz, and J. Zupan, 2012a, Phys. Rev. Lett. **109**, 141301.
Herrero-Garcia, J., T. Schwetz, and J. Zupan, 2012b, J. Cosmol. Astropart. Phys. 03, 005.
Hooper, D., J. Collar, J. Hall, D. McKinsey, and C. Kelso, 2010, Phys. Rev. D **82**, 123509.
Ibata, R., G. F. Lewis, M. Irwin, E. Totten, and T. R. Quinn, 2001, Astrophys. J. **551**, 294.
Jungman, G., M. Kamionkowski, and K. Griest, 1996, Phys. Rep. **267**, 195.
Kamionkowski, M., and S. M. Koushiappas, 2008, Phys. Rev. D **77**, 103509.
Kazantzidis, S., *et al.*, 2004, Astrophys. J. **611**, L73.
Kelso, C., D. Hooper, and M. R. Buckley, 2012, Phys. Rev. D **85**, 043515.
Kerr, F. J., and D. Lynden-Bell, 1986, Mon. Not. R. Astron. Soc. **221**, 1023.
Kim, S., *et al.* (KIMS Collaboration), 2012, Phys. Rev. Lett. **108**, 181301.
Komatsu, E., *et al.* (WMAP Collaboration), 2011, Astrophys. J. Suppl. Ser. **192**, 18.
Kopp, J., T. Schwetz, and J. Zupan, 2012, J. Cosmol. Astropart. Phys. 03, 001.

Kos, M. (DEAP/CLEAN Collaboration), 2010, Proc. Sci. ICHEP2010, 455.
Kraus, H., *et al.*, 2011, Proc. Sci., IDM2010, 109.
Kuhlen, M., M. Lisanti, and D. N. Spergel, 2012, Phys. Rev. D **86**, 063505.
Kuhlen, M., *et al.*, 2010, J. Cosmol. Astropart. Phys. 02, 030.
Kuzniak, M., M. Boulay, and T. Pollmann, 2012, Astropart. Phys. **36**, 77.
Lee, S. K., and A. H. Peter, 2012, J. Cosmol. Astropart. Phys. 04, 029.
Lewin, J., and P. Smith, 1996, Astropart. Phys. **6**, 87.
Lewis, M. J., and K. Freese, 2004, Phys. Rev. D **70**, 043501.
Lima, J., R. Silva, and A. Plastino, 2001, Phys. Rev. Lett. **86**, 2938.
Lin, S., *et al.* (TEXONO Collaboration), 2009, Phys. Rev. D **79**, 061101.
Ling, F., E. Nezri, E. Athanassoula, and R. Teyssier, 2010, J. Cosmol. Astropart. Phys. 02, 012.
Lisanti, M., and D. N. Spergel, 2012, Phys. Dark Univ. **1**, 155.
Lisanti, M., L. E. Strigari, J. G. Wacker, and R. H. Wechsler, 2011, Phys. Rev. D **83**, 023519.
Majewski, S. R., M. Skrutskie, M. D. Weinberg, and J. C. Ostheimer, 2003, Astrophys. J. **599**, 1082.
Mao, Y.-Y., L. E. Strigari, R. H. Wechsler, H.-Y. Wu, and O. Hahn, 2013, Astrophys. J. **764**, 35.
Marchionni, A., *et al.* (ArDM Collaboration), 2011, J. Phys. Conf. Ser. **308**, 012006.
Masso, E., S. Mohanty, and S. Rao, 2009, Phys. Rev. D **80**, 036009.
McCabe, C., 2010, Phys. Rev. D **82**, 023530.
McMillan, P. J., and J. J. Binney, 2009, arXiv:0907.4685.
Mignard, F., 2000, Astron. Astrophys. **354**, 522.
Monroe, J., and P. Fisher, 2007, Phys. Rev. D **76**, 033007.
Morgan, B., A. M. Green, and N. J. Spooner, 2005, Phys. Rev. D **71**, 103507.
Moriyama, S. (XMASS Collaboration), 2011, Proc. Sci., IDM2010, 057.
Natarajan, A., 2011, Adv. Astron. **2011**, 285346.
Natarajan, A., C. Savage, and K. Freese, 2011, Phys. Rev. D **84**, 103005.
Natarajan, A., and P. Sikivie, 2005, Phys. Rev. D **72**, 083513.
Newberg, H. J., *et al.* (SDSS Collaboration), 2003, Astrophys. J. **596**, L191.
Nygren, D., 2011, arXiv:1102.0815.
Pato, M., O. Agertz, G. Bertone, B. Moore, and R. Teyssier, 2010, Phys. Rev. D **82**, 023531.
Petriello, F., and K. M. Zurek, 2008, J. High Energy Phys. 09, 047.
Primack, J. R., D. Seckel, and B. Sadoulet, 1988, Annu. Rev. Nucl. Part. Sci. **38**, 751.
Purcell, C. W., J. S. Bullock, and M. Kaplinghat, 2009, Astrophys. J. **703**, 2275.
Purcell, C. W., A. R. Zentner, and M.-Y. Wang, 2012, J. Cosmol. Astropart. Phys. 08, 027.
Ralston, J. P., 2010, arXiv:1006.5255.
Read, J., G. Lake, O. Agertz, and V. P. Debattista, 2008a, arXiv:0803.2714.
Read, J. I., G. Lake, O. Agertz, and V. Debattista, 2008b, Astron. Nachr. **329**, 1022.
Reid, M., *et al.*, 2009, Astrophys. J. **700**, 137.
Roberts, M. S., and R. N. Whitehurst, 1975, Astrophys. J. **201**, 327.
Rubin, V. C., J. Ford, and W. Kent, 1970, Astrophys. J. **159**, 379.
Salucci, P., F. Nesti, G. Gentile, and C. Martins, 2010, Astron. Astrophys. **523**, A83.
Sandage, A., M. Sandage, and J. Kristian, 1975, *Galaxies and the Universe* (University of Chicago Press, Chicago).
Sanglard, V., *et al.* (EDELWEISS Collaboration), 2005, Phys. Rev. D **71**, 122002.
Savage, C., K. Freese, and P. Gondolo, 2006, Phys. Rev. D **74**, 043531.
Savage, C., K. Freese, P. Gondolo, and D. Spolyar, 2009, J. Cosmol. Astropart. Phys. 09, 036.
Savage, C., G. Gelmini, P. Gondolo, and K. Freese, 2009, J. Cosmol. Astropart. Phys. 04, 010.
Savage, C., G. Gelmini, P. Gondolo, and K. Freese, 2011, Phys. Rev. D **83**, 055002.
Savage, C., P. Gondolo, and K. Freese, 2004, Phys. Rev. D **70**, 123513.
Schnee, R., 2011, arXiv:1101.5205.
Schoenrich, R., J. Binney, and W. Dehnen, 2009, arXiv:0912.3693.
Schwetz, T., and J. Zupan, 2011, J. Cosmol. Astropart. Phys. 08, 008.
Seabroke, G., *et al.*, 2008, Mon. Not. R. Astron. Soc. **384**, 11.
Sikivie, P., 1998, Phys. Lett. B **432**, 139.
Sikivie, P., 1999, Phys. Rev. D **60**, 063501.
Sikivie, P., and J. R. Ipser, 1992, Phys. Lett. B **291**, 288.
Sikivie, P., I. Tkachev, and Y. Wang, 1997, Phys. Rev. D **56**, 1863.
Smith, M. C., *et al.*, 2007, Mon. Not. R. Astron. Soc. **379**, 755.
Smith, P., and J. Lewin, 1990, Phys. Rep. **187**, 203.
Spergel, D. N., 1988, Phys. Rev. D **37**, 1353.
Springel, V., *et al.*, 2008, Mon. Not. R. Astron. Soc. **391**, 1685.
Stadel, J., *et al.*, 2008, arXiv:0808.2981.
Stiff, D., L. M. Widrow, and J. Frieman, 2001, Phys. Rev. D **64**, 083516.
Stinson, G., *et al.*, 2010, arXiv:1004.0675.
Strigari, L. E., 2009, New J. Phys. **11**, 105011.
Tremaine, S., 1999, Mon. Not. R. Astron. Soc. **307**, 877.
Tretyak, V., 2010, Astropart. Phys. **33**, 40.
Tsallis, C., 1988, J. Stat. Phys. **52**, 479.
Tucker-Smith, D., and N. Weiner, 2001, Phys. Rev. D **64**, 043502.
Ullio, P., M. Kamionkowski, and P. Vogel, 2001, J. High Energy Phys. 07, 044.
Valluri, M., V. Debattista, T. Quinn, and B. Moore, 2009, arXiv:0906.4784.
Valluri, M., *et al.*, 2013, Astrophys. J. **767**, 93.
Vogelsberger, M., *et al.*, 2009, Mon. Not. R. Astron. Soc. **395**, 797.
Weber, M., and W. de Boer, 2010, Astron. Astrophys. **509**, A25.
Wong, H. T., and S.-T. Lin (TEXONO + CDEX Collaboration), 2010, Proc. Sci., ICHEP2010, 439.
Yanny, B., *et al.* (SDSS Collaboration), 2003, Astrophys. J. **588**, 824.
Zemp, M., O. Y. Gnedin, N. Y. Gnedin, and A. V. Kravtsov, 2012, Astrophys. J. **748**, 54.
Zwicky, F., 1937, Astrophys. J. **86**, 217.